Chapter – 5

Synthesis, Adsorption and Catalytic performance of nano Zirconium phosphate and its composite with Chitosan

5.1 Introduction

Zirconium phosphate is the most studied member of the well-known family of layered solid acids [1]. Tetravalent metal phosphates i.e., Zr/Ti/Hf phosphate is an important catalog of inorganic materials [2] and zirconium phosphate has been well studied as solid acid catalyst which exhibits excellent chemical stability, insolubility in water, fast kinetics and environment-friendly properties. Tetravalent metal acid salts have also emerged as promising adsorbent materials as they possess good ion mexchange properties, thermal stability and chemical stability. ZrP particles are reported to be promising inorganic polymer fillers that can be used either with charged or neutral polymers depending on the chemical properties of the surface of their constituting layers. The presence of P-OH groups on the surface of the layers favours the use of ZrP particles with polymers possessing polar groups (e.g. starch) whereas the surface of the layers must be organically functionalised when using ZrP particles with neutral polymers, so as to promote stronger interactions with the polymer matrix. Recently, some research groups have reported good adsorption potential of nano structured ZrP towards heavy metals, fluoride, organic compounds [3-6]. However, there are very few publications concerning the use of ZrP for the entrapment of dyes from wastewater or other sources [7-10] Two methodologies were applied for remediation of dyes: (1) the use of ZrP as a photo catalyst support in the photo catalytic degradation of dyes [7] and (2) sorption and/or intercalation of dyes in α-type ZrP [8, 9 &10]. The intercalation of malachite green (MG) in γ-zirconium phosphate (γ-ZrP) and one of its cationic surfactant forms (γ-ZrP/SUR+) has been investigated [11]. In the few instances found, α –ZrP revealed to be very efficient in decolorizing dye-containing coloured water solutions. Therefore, further investigations in this field are warranted. Incorporation of nanoparticles within a polymeric matrix may provide composites with better chemical–physicalproperties than those of the pure polymer [12-15] Qingrui Zhang et.al had investigated the adsorption of fluoride onto polystyrene encapsulated ZrP nanocomposite where they

had observed high adsorption capacities which was attributed to Donnan Membrane effect [16]. Sue et al. had investigated the synthesis and fracture behavior of Epoxy Nanocomposites based on Synthetic α-Zirconium Phosphate [17]. Rui Zhang et al had investigated the properties of polyacrylamide (PAM)/α-zirconium phosphate (α-ZrP) nanocomposite [18]. A novel glucose oxidase/chitosan/α-zirconium phosphate (GOD/chitosan/α-ZrP) ternary biocomposite was prepared by co-intercalating glucose oxidase (GOD) and chitosan into the interlayers of α-zirconium phosphate (α-ZrP) via a delamination-reassembly procedure [19]. Nanocomposite films of chitosan/α-zirconium phosphate were prepared using a casting process, with α-zirconium phosphate (α-ZrP) as nano-filler and chitosan as matrix [20]. Literature reports that amorphous gels are obtainedby the rapid addition of ion phosphate containing solutions to zirconium (IV) salt solution [21].

Later, Wu and his co-workers have synthesized porouszirconium phosphate through the post-synthesis surface reaction between mesoporous zirconium oxide, prepared by using CTAB as surfactant and phosphoric acid [22]. Very recently, Sinhamahapatra et al. have developed mesoporous zirconium phosphate by utilizing CTAB as structure directing agent in aqueous medium with pore dimensions ranging 2-3 nm, which have active acidic sites to catalyze Friedel-Craft benzylation reaction [23]. Rao et al. have developed porous zirconium phosphate, which catalyzes esterification reaction of palmitic acid with methanol to only 20% conversion. However, this zirconium phosphate when supported with WO_3 behaves as a strong acid catalyst and converts the palmitic acid to its corresponding ester more efficiently [24]. Swapan et al have developed new mesoporous zirconium oxophosphate materials through the evaporation induced self-assembly (EISA) method by using non-ionic Pluronic F127 as structure directing agent in acidic non-aqueous medium and was used as heterogeneous solid acid catalyst in biodiesel formation [25]. It is well known that group IV–VI transition metals form peroxo/hydroperoxy species on interaction with aqueous hydrogen peroxide or organic hydroperoxides [26]. Connick and McVey also clearly established that peroxo complexes of zirconium (IV) are formed [27]. These peroxo- and/or hydro peroxo species have been proposed as intermediates or active centers in several oxidation reactions. In these reactions, the active metal site acts as a reducing agent and polarizes the dioxygen bond, facilitating the bond cleavage. It can also simultaneously bind with oxygen and the substrate and then create a favorable reaction pathway for selective oxidation.

It was felt that we could make an attempt in synthesizing ZrP using an autoclave and use a biopolymer such as chitosan to form a biocomposite (CZrP) to improve its biodegradability properties. To the best of our knowledge there are no reports of Chitosan–ZrP nanocomposite used as an adsorbent and catalyst for treatment of individual and binary dye waste waters. The prepared ZrP and its bio-nanocomposites were studied for their adsorption potential towards Rhodamine-6G and the catalytic potential in degrading the dyes in the presence of H_2O_2.To put into advantage their formation of peroxy complexes.

5.2. Materials and Methods

Chitosan flakes (87.6% deacetylated and molecular weight 5.5 x 105 g/mol) from Sigma. Zirconium Oxychloride and Orthophosphoric acid purchased from Sigma Aldrich.

5.2.1. Synthesis of Adsorbent

Synthesis of Zirconium Phosphate (ZrP)

4.0 g of $ZrOCl_2 \cdot 8H_2O$ was mixed with 40.0 mL of H_3PO_4 (5.0 M) and kept under stirring condition at room temperature for 2 hrs. White Precipitates of Zirconium Phosphate is formed which was further kept in autoclave for 3 hrs. The precipitates were then centrifuged and washed with conductivity water and dried at 40ºC

Synthesis of Chitosan - Zirconium Phosphate nanocomposite (C-ZrP)

1 % Chitosan solution was prepared using acetic acid. The synthesized suspension of ZrP was added to the Chitosan solution followed by stirring at room temperature for 12 hrs which was further kept in autoclave for 3 hrs. This mixture was then centrifuged and washed using distilled water. Further it was dried at 40 °C. The dried product as then ground with a mortar and pestled into fine powders.

5.2.2. Characterization

FT-IR, TEM, XRD, Zetapotential and thermos gravimetric analysis are as per discussed in section 3.1.3 (Chapter 3) EDX and Raman analysis as per discussed in section 2.1.3 (chapter 2)

5.2.3. Preparation of dye solutions and batch sorption Experiments for single and binary mixture of dyes

The preparation of dye solutions and the batch sorption Experiments for single and binary mixture of dyes are as discussed in section 4.1.4 (chapter 4)

5.2.4. Equilibrium Sorption Studies

Adsorption isotherms were determined by the treatment of 0.05 g of adsorbents under study (ZrP and C-ZrP) with dye solution having an initial concentration varied from 100 to 1000 mg/L in a thermo stated rotary mechanical shaker. After agitation the contents of the flasks were filtered. The concentration of dye remaining in the solution was determined by Spectrophotometer. The results of experimental measurements were in the form of adsorption isotherms. Attempts were made to fit the equilibrium dye sorption isotherm data to a number of well-known models like Freundlich, Langmuir, Temkin and Halsey for the better understanding of the processes governing adsorption of dye on to the adsorbents under study (Section 4.1.5 Chapter 4). The results are shown in Table 5.1.

5.2.5. Sorption Dynamics

In order to investigate the sorption process of the dye Pseudo First order, Pseudo Second order, Intraparticle diffusion, Bangham and Liquid film diffusion models were used as kinetic models (Section 4.1.5 Chapter 4). The Values of correlation coefficients and standard deviation were used to compare the models which are shown in Table 5.2.

5.2.6. Thermodynamics of Sorption Studies

The thermodynamic parameters of the sorption process which are shown in Table 5.3 could be determined from the experimental data obtained at various temperatures as given in chapter 4 section 3.17.

5.2.7. Dye degradation experiments

The experimental procedure for degradation of dyes is discussed in section 2.1.4 (Chapter 2).

5.3 Results and Discussion

5.3. 1IR Spectra analysis

Figure 5.1.and Figure 5.2 show the IR spectral analysis of ZrP, CZrP and the dye loaded adsorbents of ZrP (ZrP-RB, ZrP-RR, ZrP-RH) and CZrP (CZrP-RB, CZrP-RR, CZrP-RH)

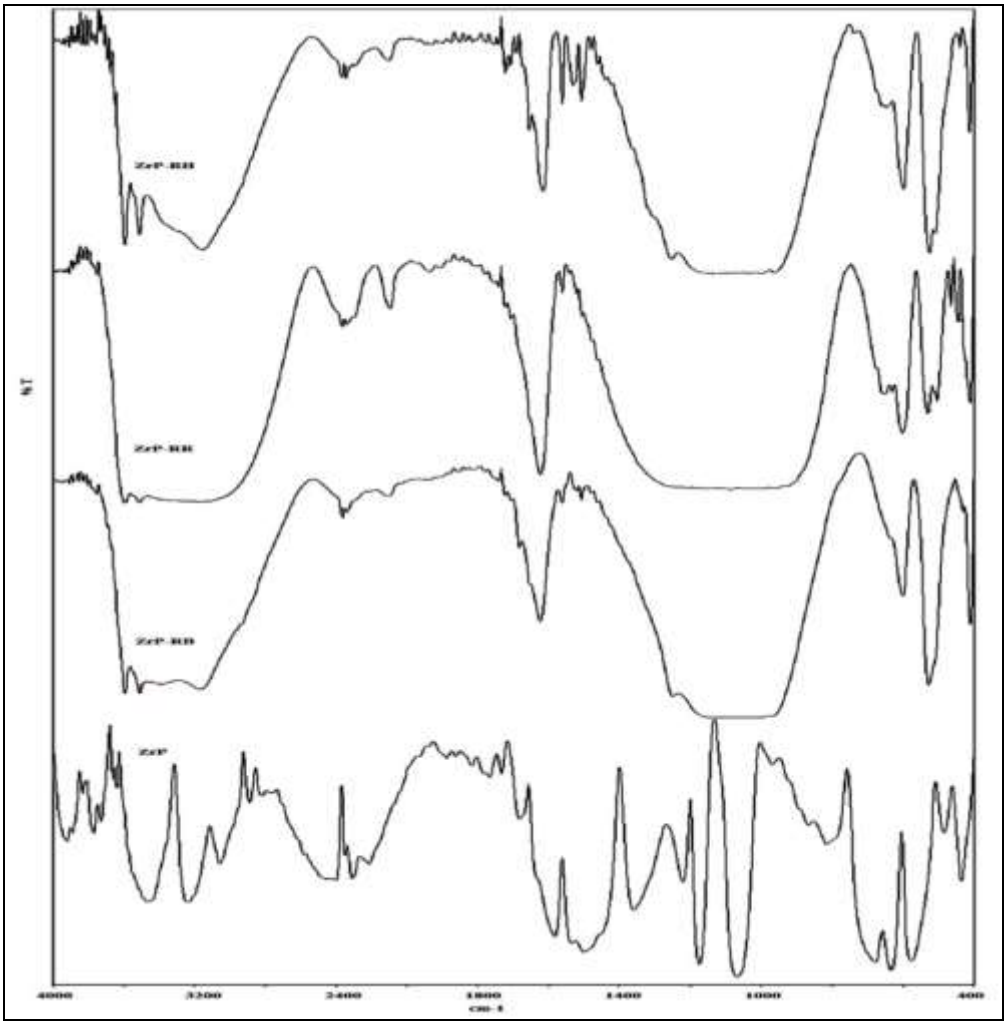

Figure 5.1 IR Spectra of ZrP, ZrP-RB, ZrP-RR and ZrP-RH

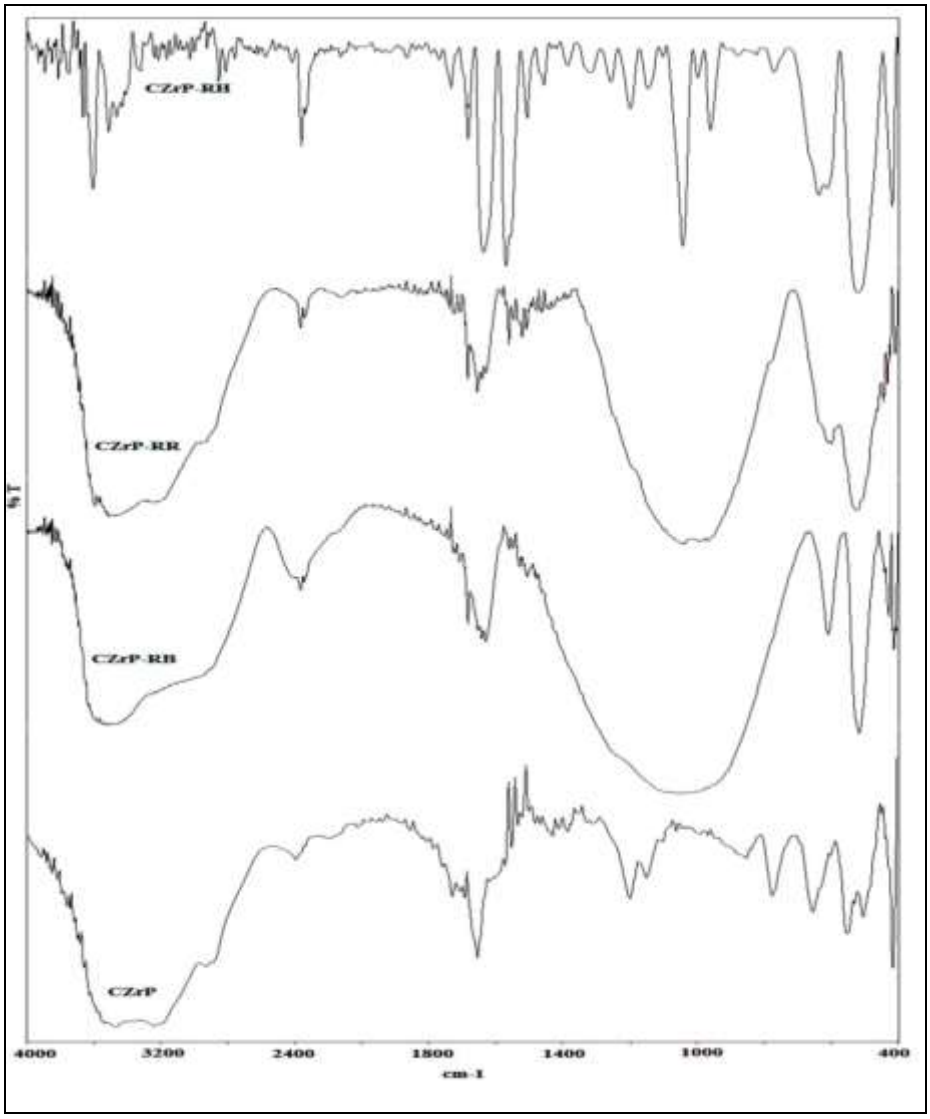

Figure 5.2 IR Spectra of CZrP, CZrP-RB, CZrP-RR and CZrP-RH

The pair of sharp bands at 3468 and 3247 cm^{-1} in ZrP has been attributed to the asymmetric O-H stretching of the water molecules, split according to site asymmetry [28]. The broad band at 3058 cm^{-1} has been assigned to the corresponding symmetric stretch, while the deformation is clearly connected to the sharp band, 1683 cm^{-1} [29]. The peaks at 1067 and 1174 cm^{-1}in ZrP and 1059, 1148 and 1197cm^{-1} for CZrP are attributed to P–OH stretching vibrations suggesting weak bronsted acid sites [30]. The sharp band at 575 cm^{-1} in ZrP and 551 cm^{-1} in CZrP are attributed to stretching and deformation vibrationof P-O bonds in PO_4^{3-}. The strong bands in the range of 950–1200 cm^{-1} are attributed to the PO_4^{3-}ν3 anti-symmetric stretching vibrations [31]. The bands at 1650 cm-1 and 1541 cm^{-1} in CZrP are attributed to C=O stretching vibration (amide-I), N-H bending vibrations (amide-II and amide-III) peaks of Chitosan. The band at 2890 and 2818 $cm^{-1}$are due to aldehydic (H-C=O) stretching vibrations. This aldehydic band of ZrP at 2890 cm^{-1} is shifted to 2392 cm^{-1} in CZrP due to zirconium (IV) doping in biopolymeric skeleton. It was observed that after adsorption of dye there is a significant shift in the O–H symmetric and asymmetric stretching frequency of ZrP and CZrP which indicates the interaction of -OH groups with the dye molecules. We did not observe protonated amine group vibrations indicating that the amine is hydrogen bonded to free hydroxide of the phosphate group [32].

5.3.2 TEM Micrographs

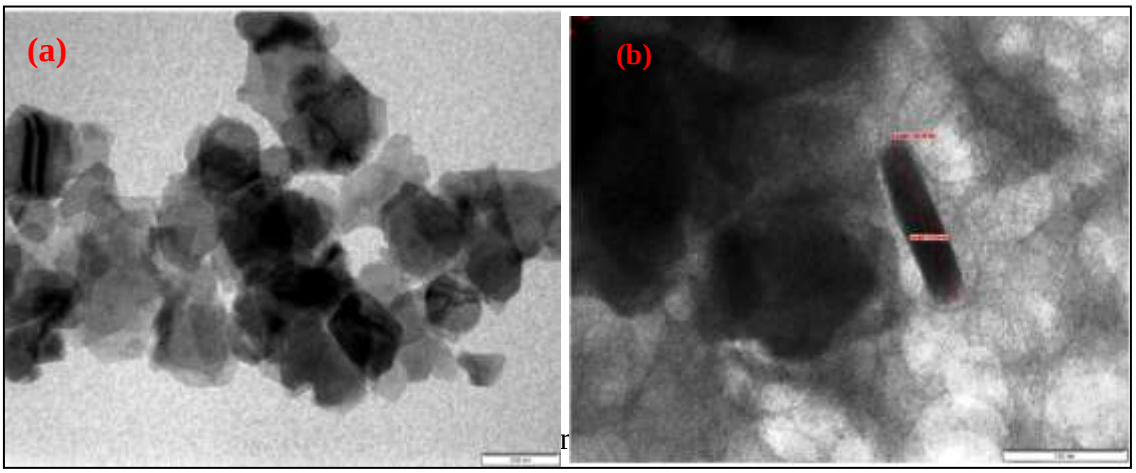

Figure 5.3 TEM Micrographs of a) ZrP and b) CZrP

Figure 5.3 a & b shows the TEM Micrographs of the ZrP Nanoparticles and CZrP nanocomposties. It is seen that α-ZrP exhibits hexagonal platy morphology with an average size of 200 nm and is exfoliated. After intercalation of Chitosan into the layers of Zirconium phosphate it is observed that some rod shaped nanocompostie with an average size of 100 nm is formed. The nanocomposite formed is fibrous in nature which provides more active sites for adsorption of dyes.

5.3.3. EDX analysis

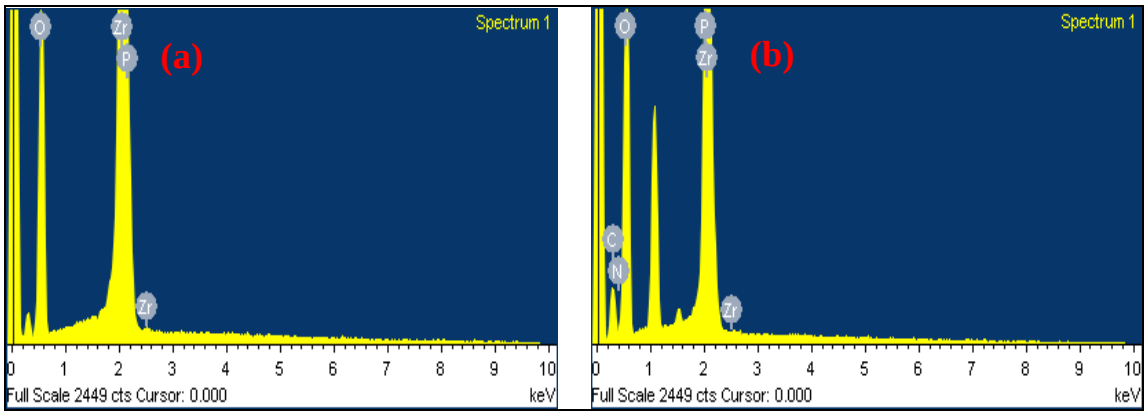

Figure 5.4 EDX spectra of a) ZrP b) CZrP

Figure 5.4 a & b shows the EDX spectra of ZrP and CZrP. The EDX analysis shows the presence of Zr and P in both ZrP and CZrP. Also the presence of N is observed in CZrP which clearly indicates that the amino groups present in chitosan are involved in intercalation with the layers of ZrP**.**

5.3.4. X-ray diffraction analysis

Figure 5.5 and Figure 5.6 shows the x-ray diffraction pattern of ZrP, CZrP and the dye loaded adsorbents of ZrP (ZrP-RB, ZrP-RR, ZrP-RH) and CZrP (CZrP-RB,CZrP-RR,CZrP-RH) typical diffraction peaks at 2θ = 11.52, 19.81, 24.34, 34.06 and 37.09° correspond to the primary diffraction of the (002), (110), (112), (206) and (116) planes of α-ZrP respectively [34]. The peak at 2θ11.52 for ZrP is weak in CZrP and also the peaks of the primary diffraction at 2θ19.81 and 24.34 for ZrP has been shifted to 2θ19.02 and 24.94 in the case of CZrP with increase in d-spacing value. The peaks of ZrP at 34.06 and 37.09 are also shifted to 34.56 and 40.96 with a decrease in d- spacing value Therefore the composite formation is both by intercalation and exfoliation mechanism. It was observed that the peaks were superimposed in the case

of dye loaded samples which indicated the dyes have been adsorbed onto the adsorbent. It is observed that after adsorption of the dyes onto ZrP and CZrP a new phase is formed with a smaller interlayer distance (0.05nm). Furthermore, several new diffraction peaks of larger interlayer distance were also seen suggesting exfoliated ZrP and CZrP nanosheets which could restack to form an ordered layered structure with an interlayer distance of ca. 9.2-9.5Å [40-48].

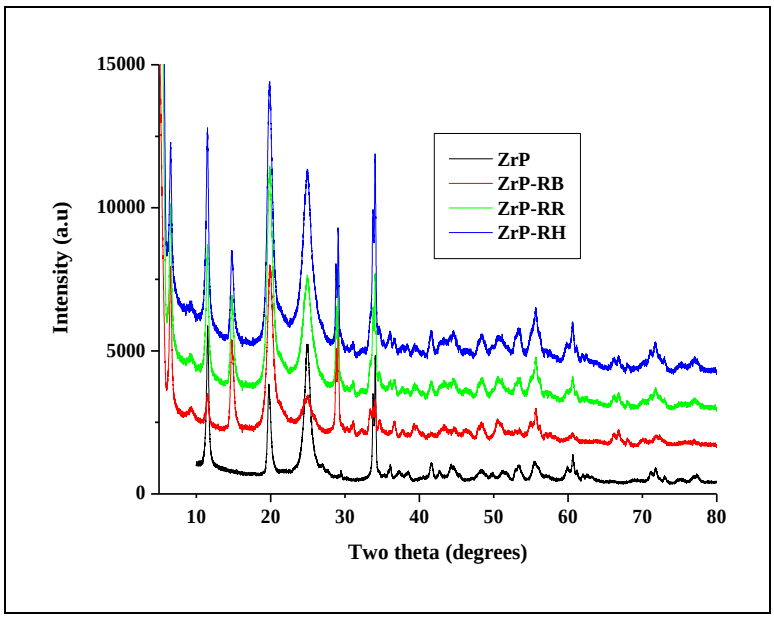

.**Figure 5.5** XRD Spectra of ZrP, ZrP-RB, ZrP-RR and ZrP-RH

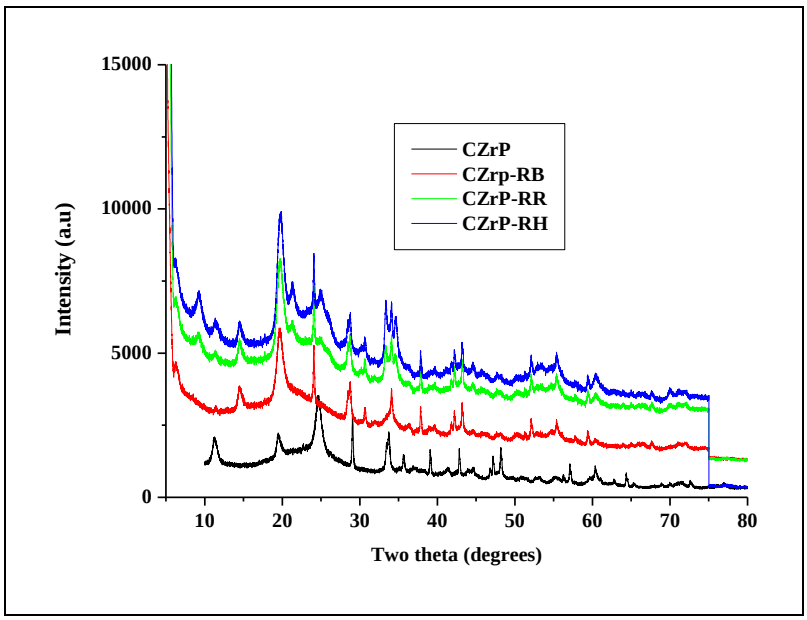

Figure 5.6 XRD Spectra of CZrP, CZrP-RB, CZrP-RR and CZrP-RH

5.3.5. Zeta potential analysis

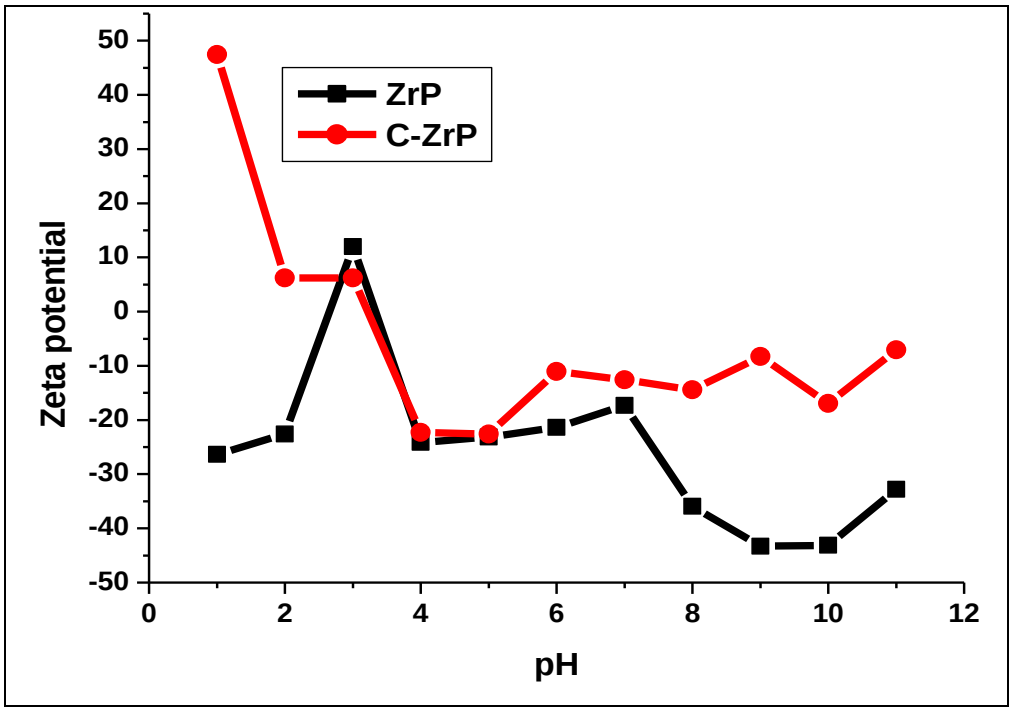

Figure 5.7 Zeta potential of ZrP and CZrP

Figure 5.7 shows the zeta potential measurements were done to determine the surface charge densities.The surface charge for ZrP is positive at acidic pH and as the pH increases the surfacecharge becomes negative. For CZrP the surface charge is positive only at pH 3 and beyond pH 3 the surface charge is negative. The zeta potential value was -15 and -20 mV for ZrP and CZrP respectively.

5.3.6. Thermogravimetric analysis

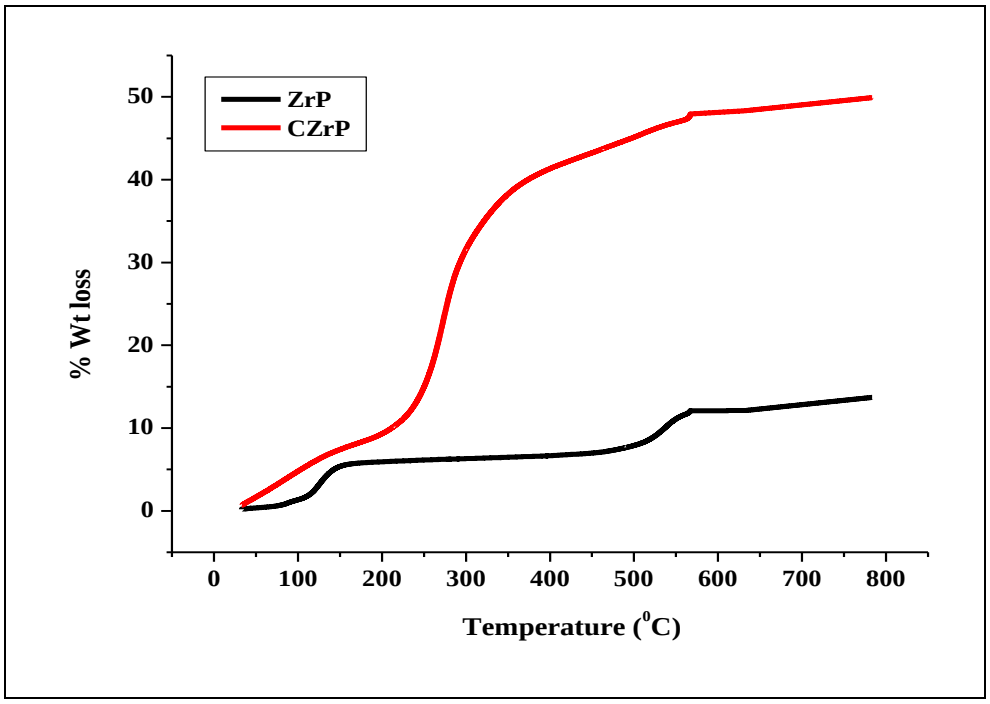

Figure 5.8 TGA of ZrP and CZrP

Figure 5.8 shows the thermogravimetric analysis of ZrP and CZrP. The total weight loss for ZrP was found to be ~ 10-12% while for CZrP the weight loss was ~48-50%. The first weight loss of 5-6% in ZrP and CZrP at 50-150 ^{0}C corresponds to loss of adsorbed moisture. The further weight loss of about 9-15% at 150^{0}C - 230^{0}Cin CZrP is due to unbounded chitosan may be present in the composite. The weight loss from 200^{0}C - 500^{0}Cin ZrP might be due to the condensation of hydroxyl groups.

5.3.7. Raman Spectroscopy analysis

The Raman spectrum (Figure 5.9) of ZrP and CZrP is characterized by a very intense band at 975 cm^{-1} which could be assigned to the symmetric stretching vibration of the PO_4^{3-}. The band located at 1049 cm^{-1} could be due to asymmetric stretching vibration of the PO_4^{3-} . The bands at 547cm^{-1} is assigned to the out ofplane bending modes of the PO_4^{3-} units present in ZrP and CZrP [49, 50]. The modes due to translational vibrations of the Zr^{4+} and PO_4^{3-} ions and the rotational vibrations of the PO_4^{3-} ions were too weak to be observed.

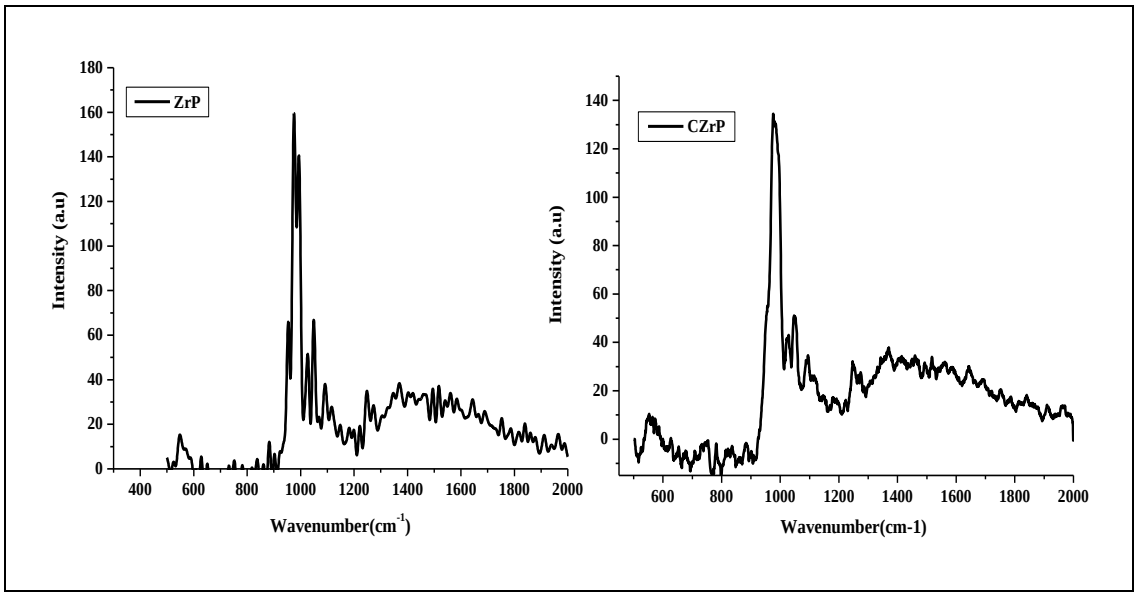

Figure 5.9 Raman spectrums of ZrP and CZrP

5.3.8 Dye adsorption studies of single component dye systems

Effect of pH

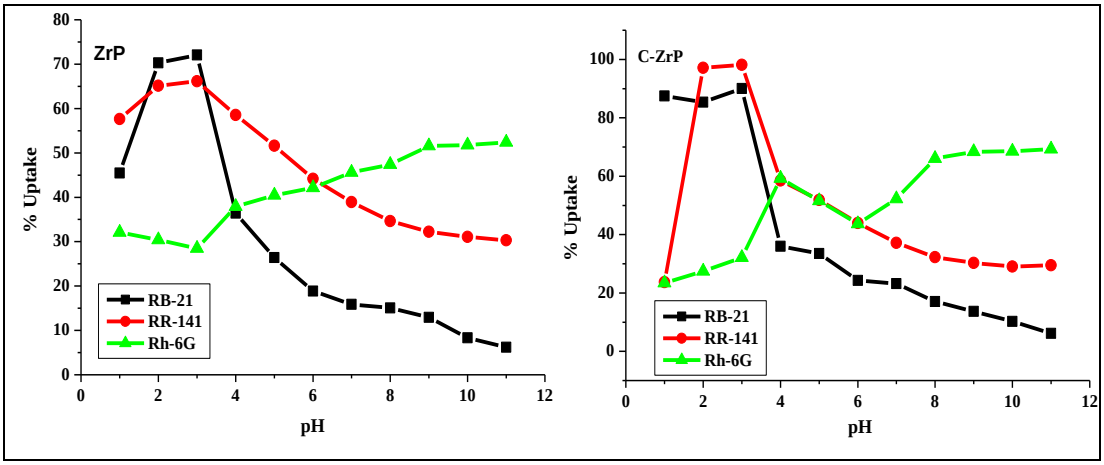

Operating parameters: 180 rpm, 100 ppm of dye, 0.05g adsorbent, time 210 min, temperature 30^0C,

Figure 5.10 Effect of pH on % uptake of RB-21, RR-141 and RH-6G onto ZrP and CZrP

Surface charge is the most important parameter for the adsorption dye molecules and is primarily affected by the solution pH. In this study, the effect of solution pH on the adsorption of dyes was investigated in the range 1 to 11, while initial concentration and temperature were kept constant. The results in figure5.10 indicate maximum adsorption for RB-21and RR-141 is observed at acidic pH (pH 2 and 3) for ZrP and CZRP while for Rh-6G (pH10)maximum adsorption took place at basic pH for both ZrP and CZrP which is in accordance with their surface charges at the respective pH values as seen from Zpc measurements.

Effect of temperature

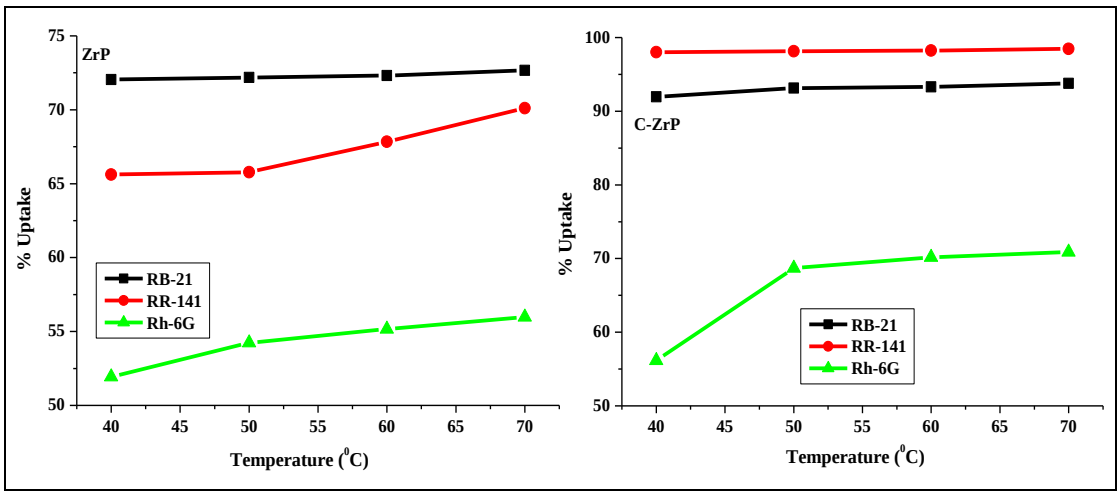

Operating parameters: 180 rpm, 100 ppm of dye, 0.05g adsorbent, time210 min

Figure 5.11 Effect of temperature on % uptake of RB-21, RR-141 and Rh-6G onto ZrP and CZrP

Adsorption of RB-21 remained unaffected onto ZrP and CZrP with respect to temperature (figure 5.11). The adsorption percentage of RR-141 slightly increased with respect to temperature in the case of ZrP while in the case of CZrP the adsorption process was not affected with increase in temperature. It was observed that adsorption of Rh-6G onto ZrP and CZrP increases with respect to temperature indicating the mechanism to be endothermic.

Effect of adsorbent dose.

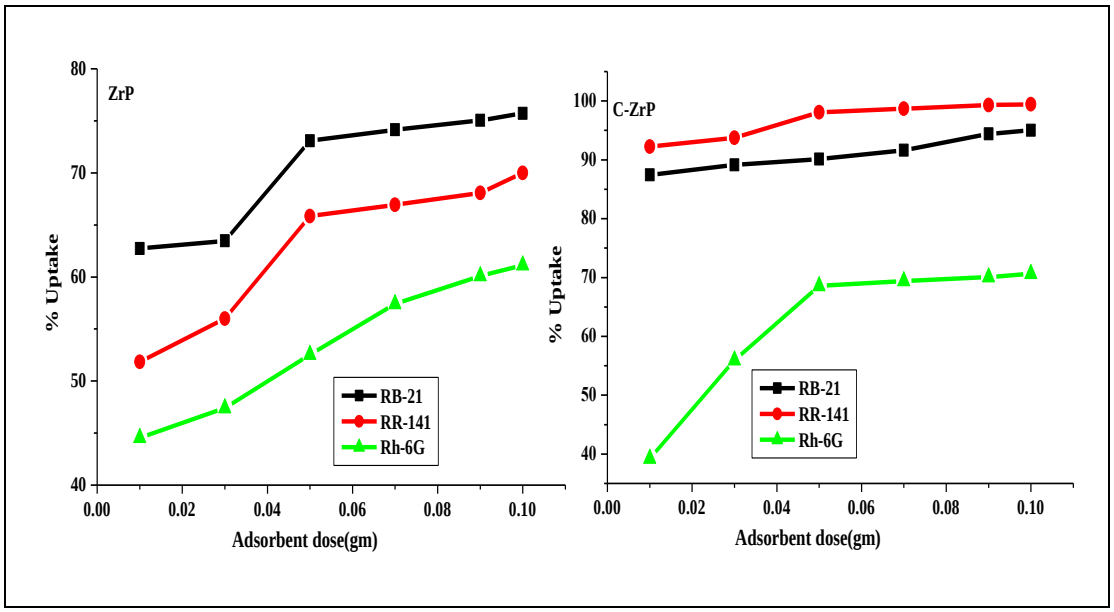

Operating parameters: 180 rpm, 100 ppm of dye, 0.05-0.1g adsorbent, time210 min, temperature 30^0C

Figure 5.12 Effect of adsorbent dose on % uptake of RB-21, RR-141 and RH-6G onto ZrP and CZrP

It is observed that saturation limit is reached at 0.05 g (Figure 5.12) for the dyes in all the three dyes. Increase in the percentage uptake of dyes with adsorbent dosage could be attributed to increase in the adsorbent surface area and hence the adsorption sites available for adsorption and almost a saturation limit are reached at 0.05 g after which it remains constant.

Effect of concentration

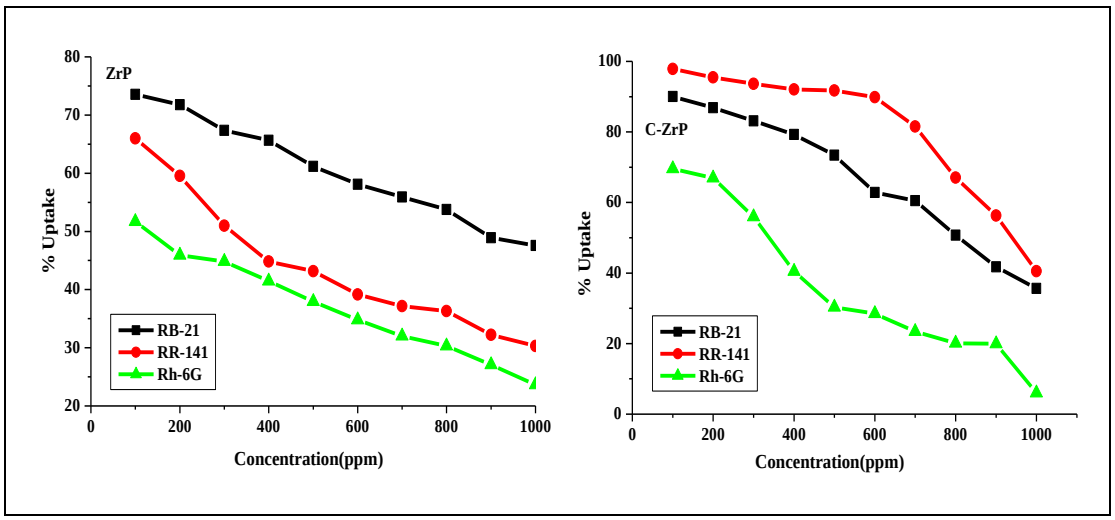

Operating parameters: 180 rpm, 100-1000 ppm of dye, 0.05g adsorbent, time 210 min, temperature 30^0C

Figure 5.13 Effect of concentration on % uptake of RB-21, RR-141 and Rh-6G onto ZrP and CZrP

It is found that the percentage uptake was found to decrease with increase in concentration (figure 5.13) for all the three dyes onto ZrP and CZrP suggesting limiting number of adsorption sites available for adsorption at higher concentration of adsorbate molecules which may be attributed to the increase in the concentration gradient and thus indicating the saturation of sorption sites. At low concentrations, the ratio of surface active sites of sorbent are more than the total sorbate components and hence may interact with the sorbent and be removed from the solution.

Sorption isotherm

The isotherm models of Freundlich, Langmuir, Temkin, and Halsey models were studied and isotherm constants for the sorption of RB-2, RR-141 and Rh-6G by ZrP and CZrP are presented in Table 5.1.The adsorption data shows that both ZrP and CZrP gave reasonably high correlation coefficient values for all the models studied. The Freundlich constant, n > 1 implies that the adsorption intensity is favorable over the entire range of concentrations studied. The fitting of Langmuir showed that the correlation coefficient values were best fitted and the calculated q_m values were in

good correlation with $q_e$exp values. The fitting of Temkin model indicated favourable adsorption for all range temperature in the case of ZrP and CZrP which is clearly shown by the temkin adsorption potential and the heat of sorption energy. The high regression values for Halsey model suggested multilayer adsorption [61]. Figure 5.14 (a, b & c) and 5.15 (a, b & c) shows the linear fit for isotherms of RB, RR and RH onto ZrP and CZrP.

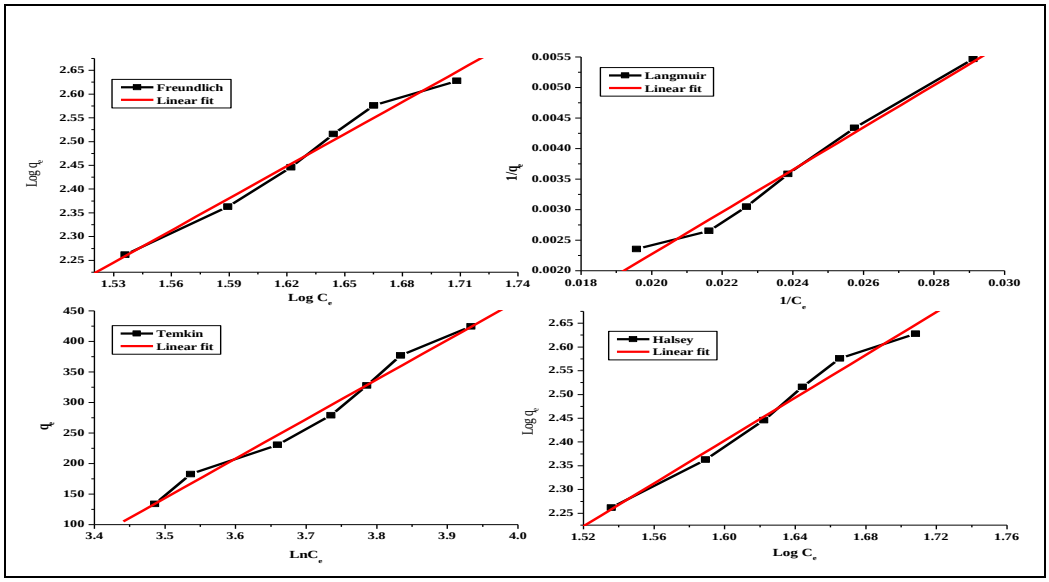

Operating parameters: 180 rpm, 100 ppm of dye, 0.05g adsorbent, time 210 min, temperature 30^0C, optimum pH

Figure 5.14 a. Linear fit of isotherm for RB onto ZrP

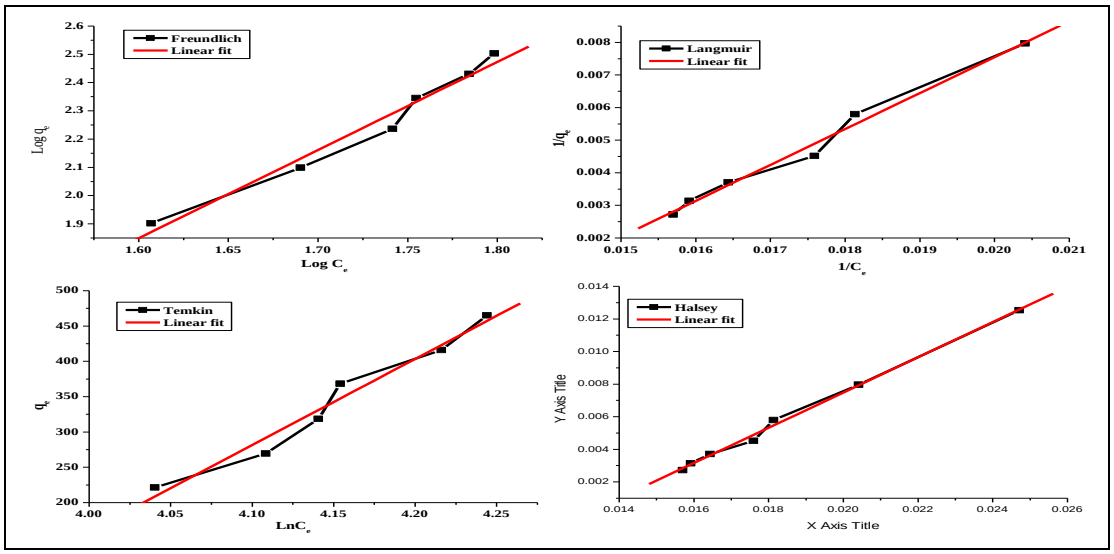

Operating parameters: 180 rpm, 100 ppm of dye, 0.05 g adsorbent, time210 min, temperature 30^0C, optimum pH

Figure 5.14 b Linear fit of isotherm for RR onto ZrP

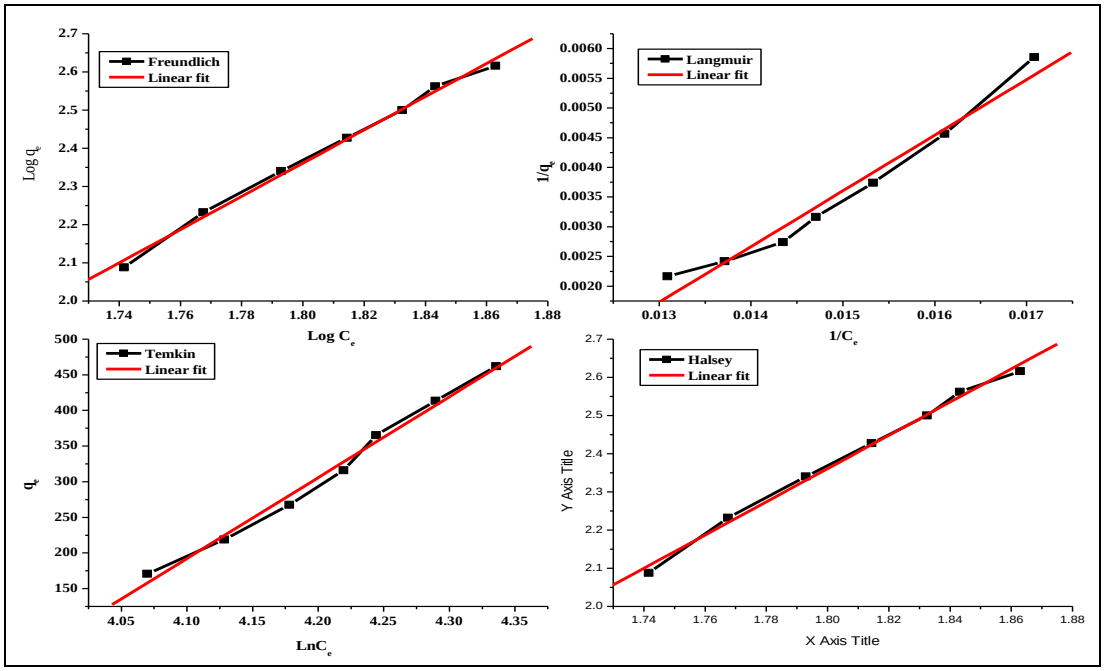

Operating parameters: 180 rpm,100 ppm of dye, 0.05 g adsorbent, time 210 min, temperature 30^{0}C, optimum pH

Figure. 5.14 c. Linear fit of isotherm for RH onto ZrP

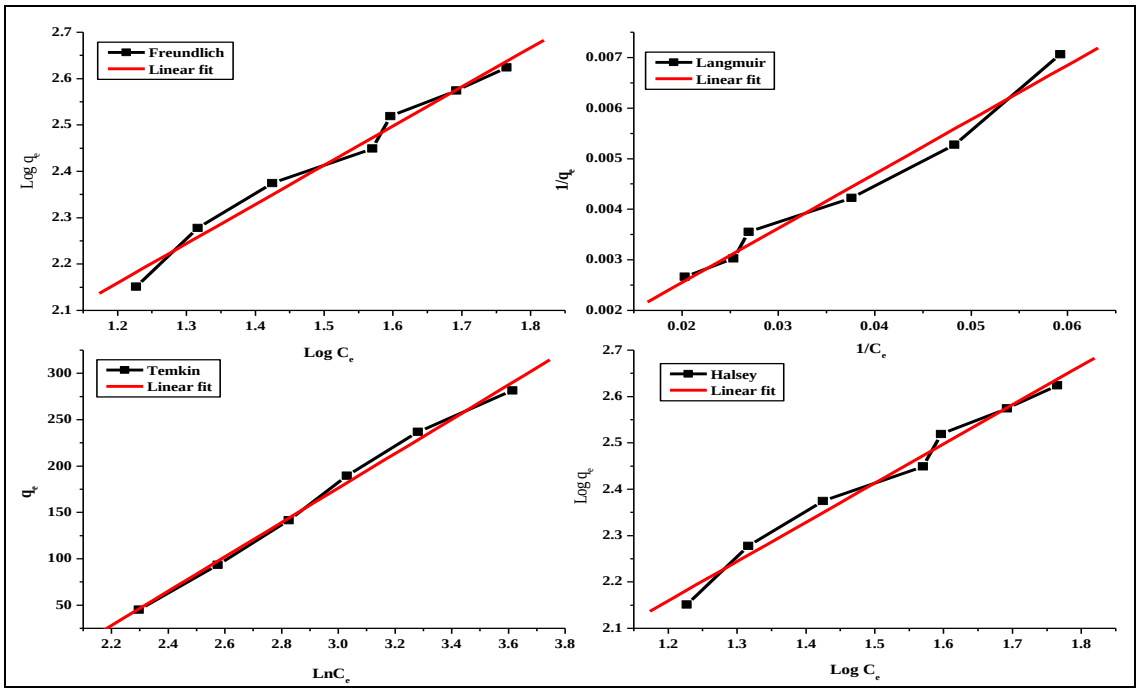

Operating parameters: 180 rpm, 100 ppm of dye, 0.05g adsorbent, time 210 min, temperature 30^{0}C, optimum pH

Figure 5.15 a. Linear fit of isotherm for RB onto CZrP

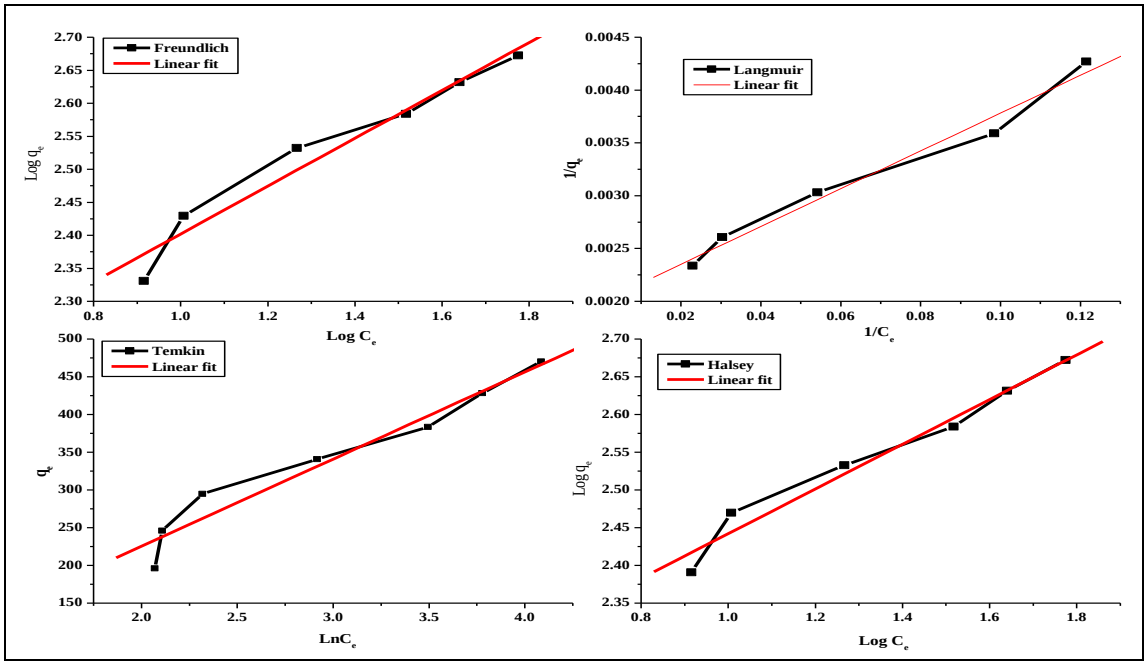

Operating parameters: 180 rpm, 100 ppm of dye, 0.05g adsorbent, time210 min, temperature 30^0C, Optimum pH

Figure 5.15 b Linear fit of isotherm for RR onto CZrP

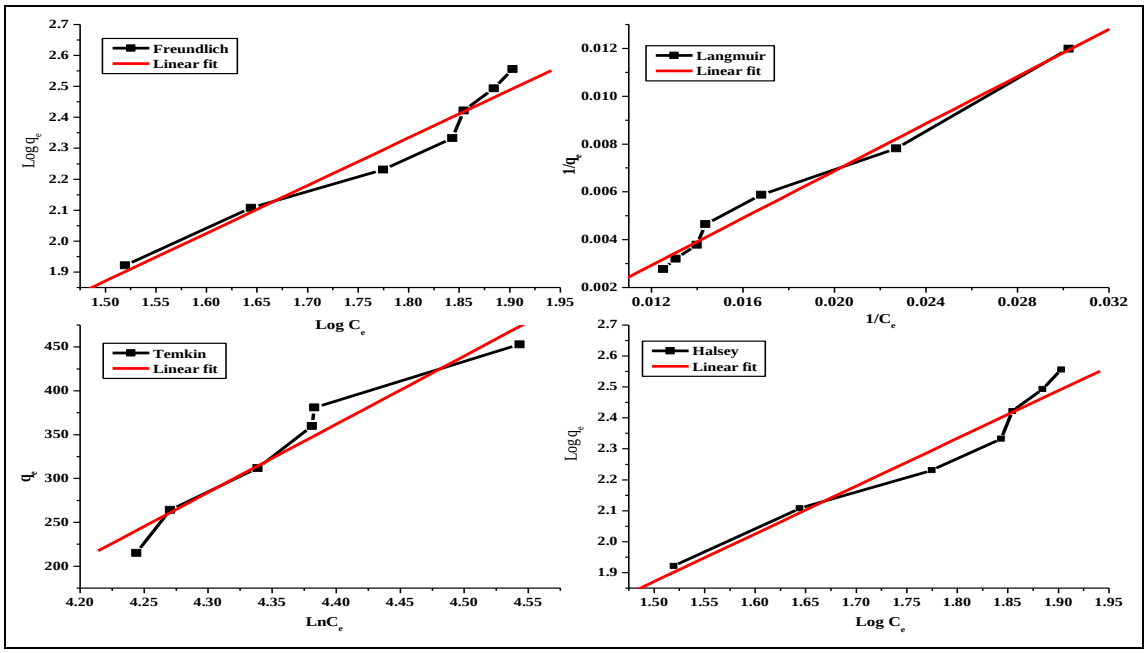

Operating parameters: 180 rpm, 100 ppm of dye, 0.05g adsorbent, time 210 min, temperature 30^0C, optimum pH

Figure 5.15c Linear fit of isotherm for RH onto CZrP

Table 5.1 Isotherms

	ZrP			**C-ZrP**		
	RB	**RR**	**RH**	**RB**	**RR**	**RH**
Freundlich						
q_e(exp) ($mg.g^{-1}$)	424.77	465.15	413.80	467.80	470	467
K_F **($L.g^{-1}$)**	3.765	2.378	5.210	13.955	10.950	13.630
N	2.253	3.119	2.352	1.182	2.758	1.838
R^2	0.991	0.987	0.997	0.990	0.978	0.976
SD	0.019	0.039	0.015	0.025	0.029	0.053
Langmuir						
q_m($mg.g^{-1}$)	423.728	409.014	433.651	457	435.161	438.596
K_L($L.mmol^{-1}$)	0.006	0.002	0.0024	0.002	0.1285	0.00462
R^2	0.991	0.993	0.9834	0.98819	0.989	0.991
SD	1.71E-04	2.59E-04	2.61E-04	0.0002	1.32E-04	4.55E-04
Temkin						
β_T	647.106	1219.54	1135	185.24	115.43	777.695
K_T ($L.mmol^{-1}$)	0.037	0.02087	0.019629	0.128947	0.954	0.019554
R^2	0.991	0.9836	0.9951	0.99709	0.975	0.96811
SD	14.681	18.381	11.369	7.561	23.935	23.923
Halsey						
K_{FH} **($L.g^{-1}$)**	0.533	1.0072	1.257	1.353	2.8668	2.0855
n_{FH}	0.443	0.320	0.229	1.182	2.758	1.838
R^2	0.991	0.987	0.997	0.990	0.978	0.976
SD	0.019	0.039	0.015	0.0256	0.029	0.053

Sorption Kinetics.

The kinetic models Pseudo First order, Pseudo Second order, Intraparticle diffusion, Bangham, Elovich and Liquid film diffusion models were studied and the kinetic constants for the sorption of RB-21, RR-141 and Rh-6G by ZrP and CZrP are presented in Table 5.2.Figure. 5.16 (a, b& c) and 5.17 (a, b & c) shows the linear fit for isotherms of RB-21, RR-141 and Rh-6G onto ZrP and CZrP. The correlation coefficients for pseudo second order model were found to be greater than the other kinetic models for ZrP and CZrP and the calculated equilibrium adsorption capacity values were closer to those obtained experimentally. This supported the assumption behind the model that the surface complexation may be the rate-limiting step involving valence forces through sharing or exchanging of electron between adsorbent and adsorbate. The plot of qt versus t1/2 did not pass through origin suggesting that intraparticle diffusion was not the only rate-controlling step but some degree of the boundary layer diffusion also controlled the adsorption process and thus the overall rate of the dye adsorption process appeared to be controlled by more than one-step The lower linear coefficient values of Liquid film diffusion model suggested that the adsorption the flow of flow of the reaction from the bulk liquid to the surface of the adsorbent is comparatively less which is also observed from the rate constant values. Also the linear coefficient values of the Bangham model suggests that the diffusion of dye molecules onto the pores of the adsorbent is less as the adsorbent is less porous and so the the rate of reaction is not controlled by diffusion of the adsorbate into the pores of the adsorbent.

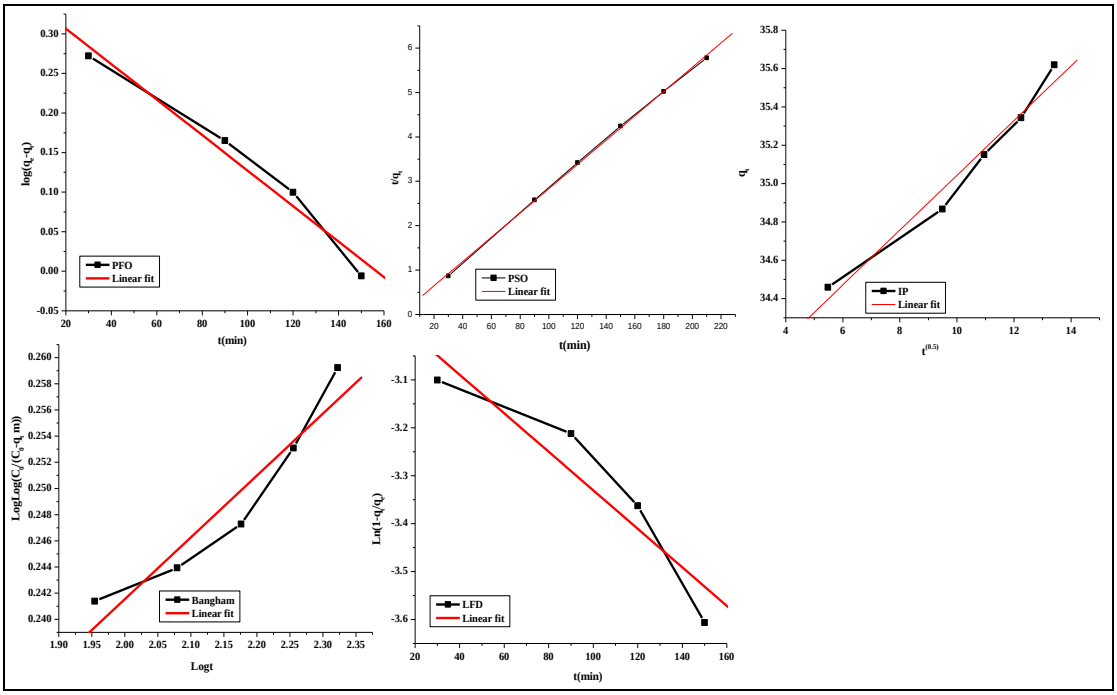

Operating parameters: 180 rpm, 100 ppm of dye, 0.05 g adsorbent, time 210 min, temperature 30^0C, optimum pH-2

Figure 5.16 a Linear fit of Kinetics for RB onto ZrP

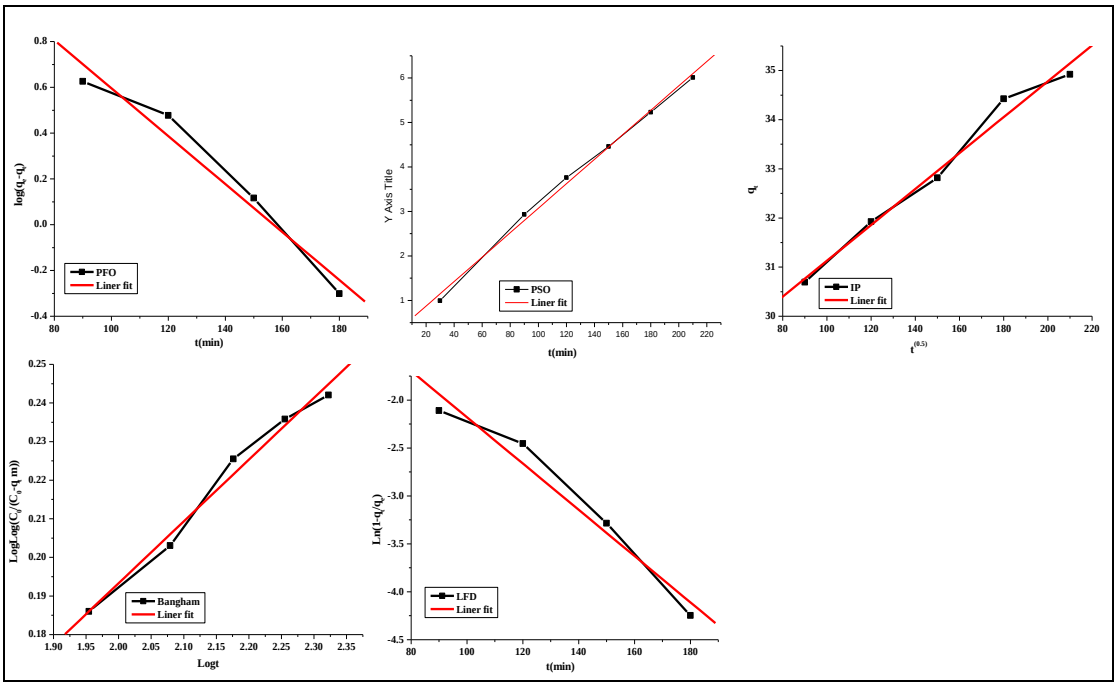

Operating parameters: 180 rpm, 100 ppm of dye, 0.05g adsorbent, time 210 min, temperature 30^0C, optimum pH-2

Figure 5.16 b. Linear fit of Kinetics for RR onto ZrP

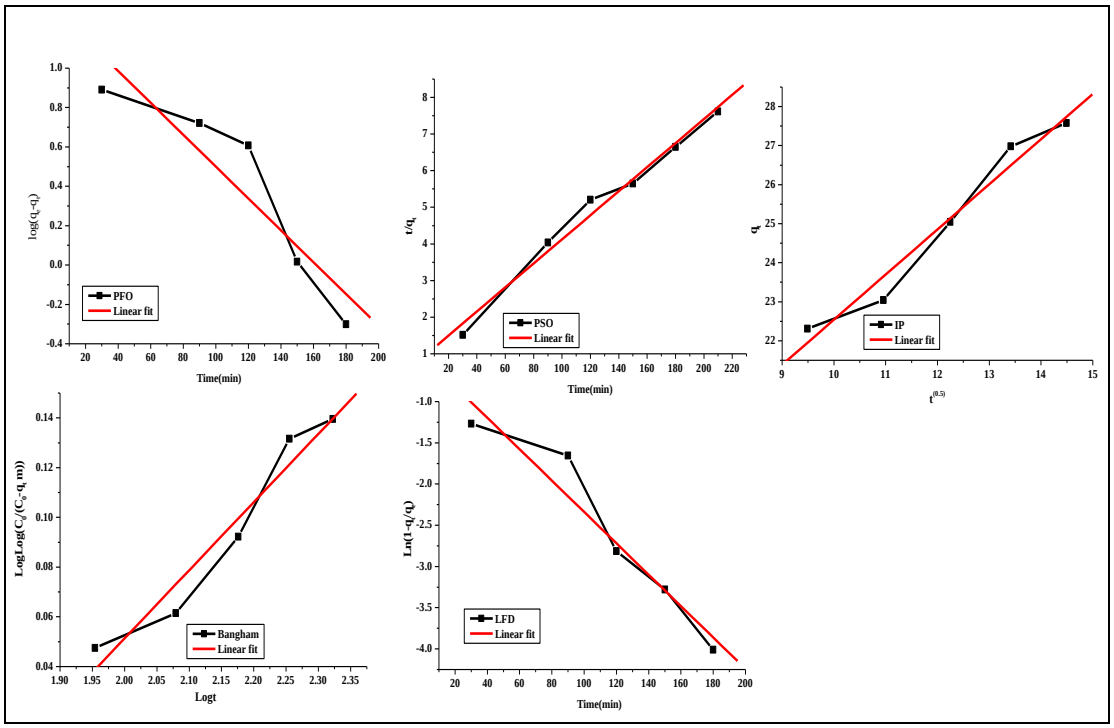

Operating parameters: 180 rpm, 100 ppm of dye, 0.05 g adsorbent, time 210 min, temperature 30^0C, optimum pH-10

Figure 5.16 c Linear fit of Kinetics for RH onto ZrP

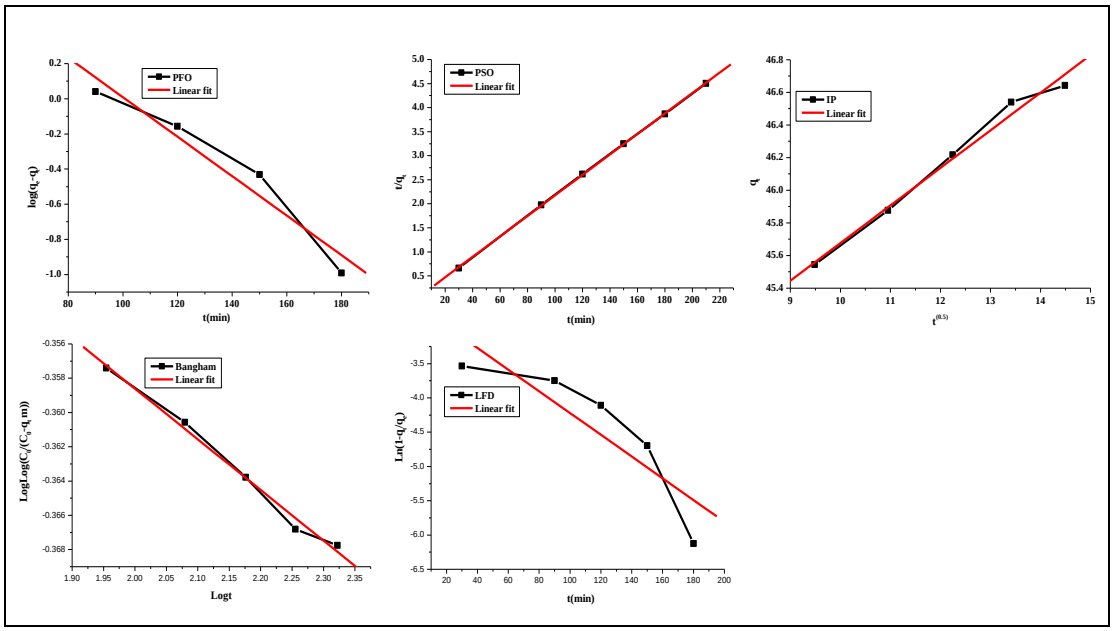

Operating parameters: 180 rpm, 100 ppm of dye, 0.05 g adsorbent, time 210 min, temperature 30^0C, optimum pH-2

Figure 5.17 a. Linear fit of Kinetics for RB onto CZrP

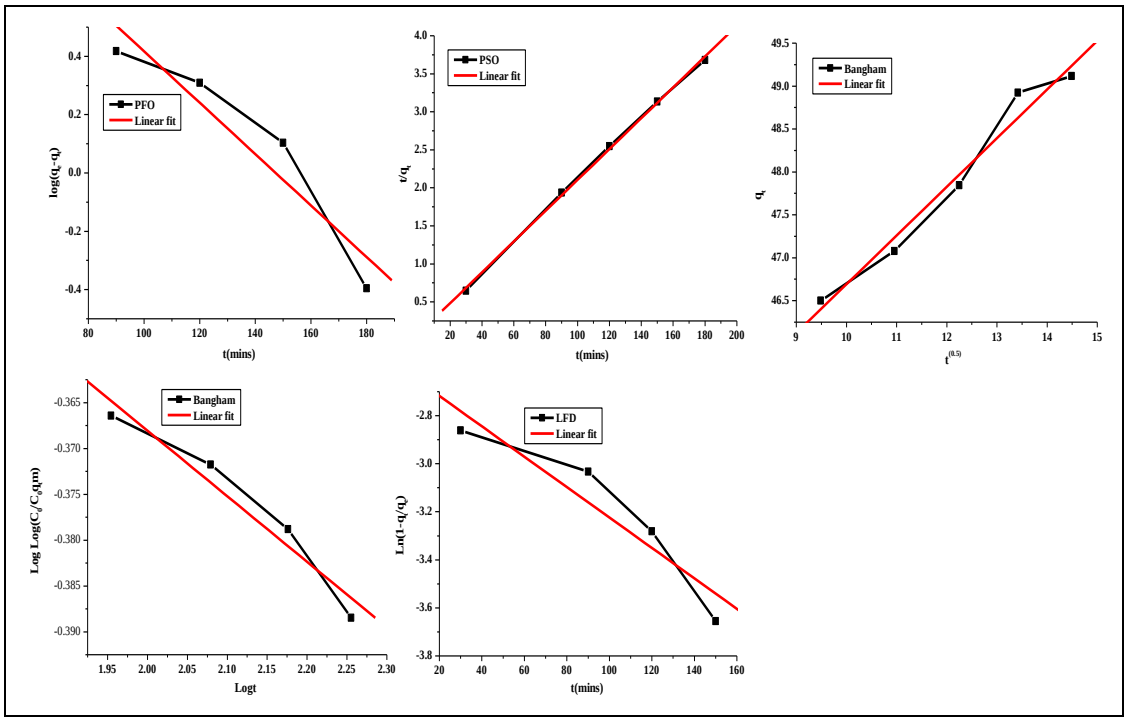

Operating parameters: 180 rpm, 100 ppm of dye, 0.05 g adsorbent, time 210 min, temperature 30^0C, optimum pH-2

Figure 5.17 b. Linear fit of Kinetics for RR onto CZrP

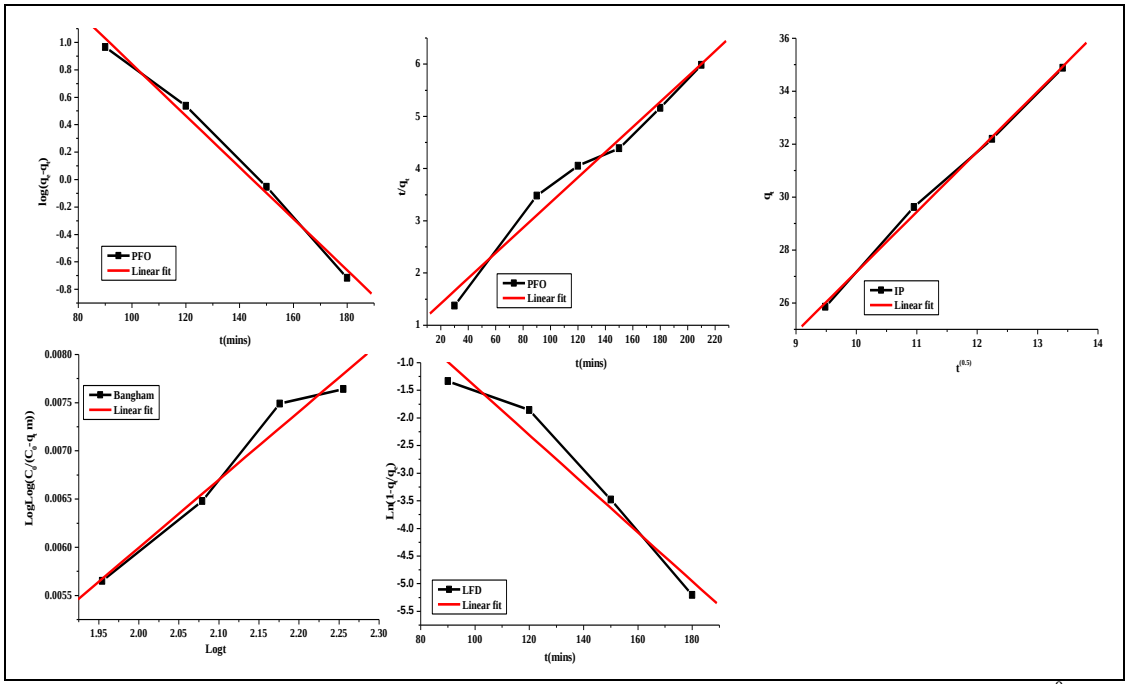

Operating parameters: 180 rpm, 100 ppm of dye, 0.05 g adsorbent, time210 min, temperature 30^0C, optimum pH-10

Figure 5.17 c Linear fit of Kinetics for RH onto CZrP

Table 5.2 Kinetics

Kinetics	ZrP			C-CZrP		
	RB	RR	RH	RB	RR	**RH**
Pseudo first order						
q_e (exp) ($mg.g^{-1}$)	36.329	34.923	27.580	46.642	49.911	35.080
q_e($mg.g^{-1}$)	22.463	44.064	20.373	13.573	19.928	16.548
K_1(min^{-1})	0.0051	0.024	0.0186	0.025	0.0203	0.0432
r^2	0.9859	0.9811	0.922	0.970	0.947	0.995
SD	0.0238	0.0979	0.225	0.132	0.141	0.084
Pseudo second order						
q_e	36.360	36.401	30.450	46.970	49.309	41.373
K_2($g.mgmin^{-1}$)	0.0074	0.0004	0.001	0.0102	0.005	0.0006
r^2	0.999	0.997	0.991	0.999	0.999	0.987
SD	0.0050	0.132	0.306	0.017	0.046	0.280
Intraparticle diffusion						
K_{ip}($mg.gmin^{-0.5}$)	0.142	0.036	1.156	0.230	0.566	2.273
r^2	0.985	0.991	0.98	0.992	0.985	0.998
SD	0.088	0.269	0.505	0.062	0.223	0.235
Bangham						
K_b	8.456	7.301	28.596	17.242	12.959	11.982
A	0.047	0.160	0.274	0.029	0.7149	0.0070
r^2	0.953	0.991	0.972	0.995	0.9730	0.982
SD	0.002	0.003	0.011	4.94E-04	0.002	2.16E-04
Liquid film diffusion						
K_{fd}	0.0040	0.024	0.018	0.015	0.006	0.044
r^2	0.940	0.981	0.919	0.881	0.940	0.977
SD	0.091	0.225	0.395	0.567	0.143	0.452

Thermodynamic studies

The negative values of ΔG and ΔH as in Table 5.3indicate the thermodynamically feasiblespontaneous nature of adsorption and increase in gibbs energy. The negative value of enthalpy change indicated that the adsorption wasphysical in nature involving strong forces of attraction and is exothermic. The negative ΔS values indicate a reduction of randomness at the solid–liquid interface during the adsorptionprocess. Therefore the adsorption might be due to physical or chemical adsorption where the values of ΔH ranges from -4 to -40 KJ.mol^{-1} whereas for chemical adsorption the values fall in the range of -40 to 800 40 KJ.mol^{-1}

Table 5.3 Thermodynamic parameters

Thermodynamic parameters					
ΔG(KJ/mol)					
	303K	**313K**	**323K**	**333K**	**343K**
	ZrP				
RB	-14893.6	-15385.1	-15876.6	-16368.2	-16859.7
RR	-13331	-13770.9	-14210.9	-14650.9	-15090.8
RH	-10469.1	-10814.7	-11160.2	-11505.7	-11851.2
	CZrP				
RB	-12126	-12526.2	-12926.4	-13326.6	-13726.8
RR	-23817.6	-23817.6	-23817.6	-23817.6	-23817.6
RH	-12108.1	-12507.7	-12907.3	-13306.9	-13706.5

	ZrP		**CZrP**	
	ΔH (KJ/mol)	ΔS (J/molK)	ΔH (KJ/mol)	ΔS (J/molK)
RB	-1.34E-05	-49.1537	-2.60E-05	-40.0198
RR	-1.95E-05	-43.99664	-5.66E-05	-78.606
RH	-1.85E-05	-34.55165	-1.14E-05	-39.9606

5.3.9. Dye adsorption studies of binary dye systems

It is well known that extensive research has been carried out for adsorption of anionic and cationic dyes. But the effluents discharged from industries are mixture of more than one or more dyes. Multi-component equilibrium studies dealt with competitive adsorption and only a fewwere concerned with the selectivity of adsorption processes. Extensions of several common isotherms were used tomodel the experimental data, namely, the extended Langmuir equation and Jain and Snoeyink modified extended Langmuir model. The models are discussed in section 3.28 (chapter 3). Table 5.4 and 5.5 shows the isotherm models for binary mixture.

Therefore investigation has been carried out for adsorption of mixture of dyes onto ZrP and CZrP. Table 5.4 shows theqm, K_l and $a_L$for binary systems. Table 5.5 shows the parameters of Jain and Snoeyink modified extended Langmuir model. Figure 5.18 (a, b & c) and Figure 5.19 (a, b & c) shows the linear fit for isotherms of RB+RR, RB+RH and RB+RR onto ZrP and CZrP. The extended Langmuir fitted well into the sorption isotherm of binary mixtures. It was observed that the adsorption capacity of binary mixture was less on comparison to single component due to the competitive adsorption of dye molecules onto the active sites of the adsorbent. However the decrease in efficiency was on an average less than 20% for all three binary mixtures using ZrP and CZrP. P factor model was also used to simulate the competitive sorption behavior of mixture of dyes in bi-solute system. This model assumed a simplified approach to compare and correlate single-solute sorption with those of the multi-component systems by introducing a ‘‘lumped’’ capacity factor Pi. The P-factor is defined as the ratio between the monolayer capacities in single- and multi-solute systems. In all the three mixture of dyes the value of P greater than unity indicating confirming that sorption was hindered by the presence of competing dye in the binary mixture.

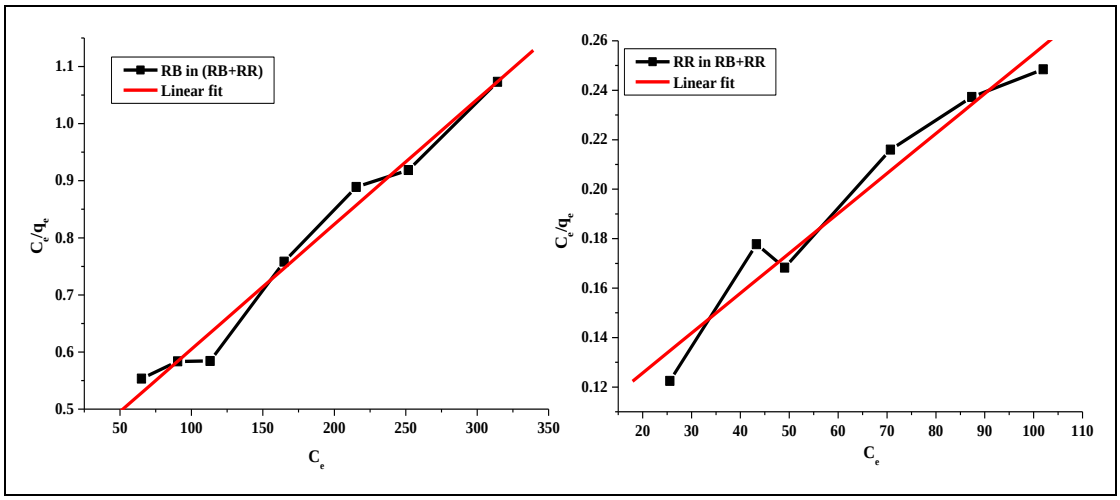

Operating parameters: 180 rpm, 100 ppm of dye, 0.05 g adsorbent, time 210 min, temperature 30^0C, optimum pH-3

Figure 5.18 a. Linear fit of isotherm for RB and RR in (RB+RR) onto ZrP

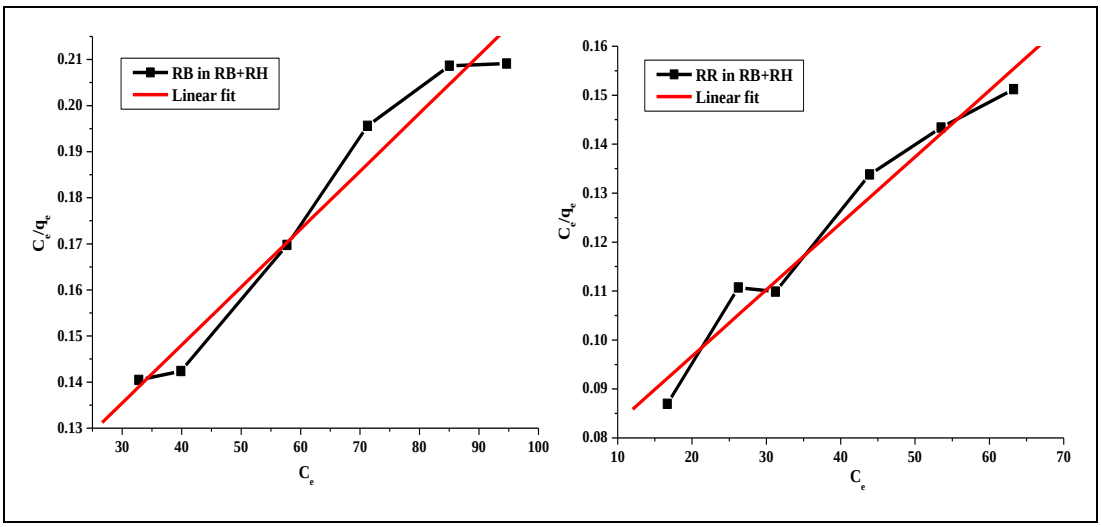

Operating parameters: 180 rpm, 100 ppm of dye, 0.05g adsorbent, time 210min, temperature 30^0C, optimum pH-8

Figure 5.18.b. Linear fit of isotherm for RB and RH in (RB+RH) onto ZrP

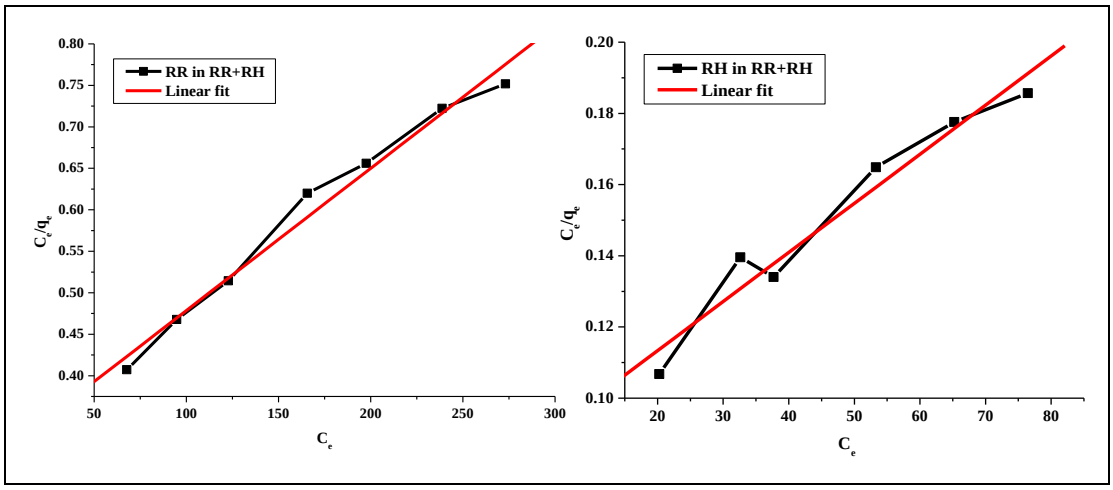

Operating parameters: 180 rpm, 100 ppmof dye, 0.05g adsorbent, time 210 min, temperature 30^0C, optimum pH-9

Figure 5.18 c. Linear fit of isotherm for RR and RH in (RR+RH) onto ZrP

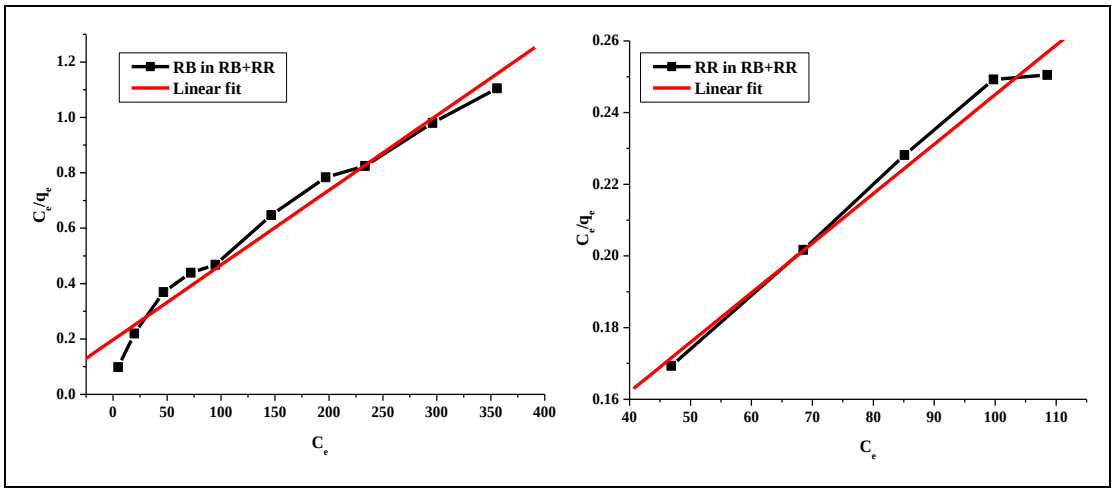

Operating parameters: 180 rpm, 100 ppm of dye, 0.05g adsorbent, time 210 min, temperature 30^0C, optimum pH-3

Figure 5.19 a. Linear fit of isotherm for RB and RR in (RB+RR) onto CZrP

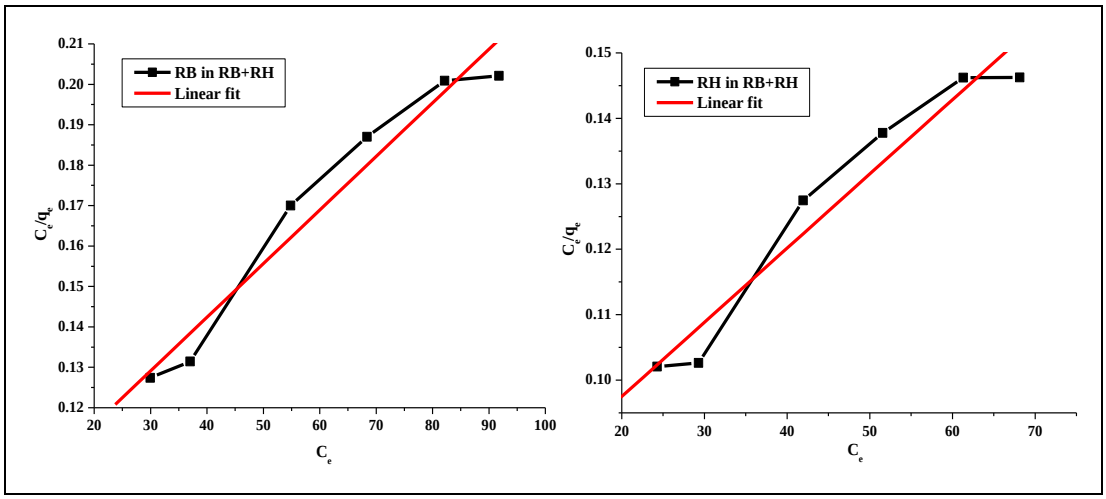

Operating parameters: 180 rpm, 100 ppm of dye, 0.05g adsorbent, time 210 min, temperature 30^0C, optimum pH-8

Figure 5.19 b. Linear fit of isotherm for RB and RH in (RB+RH) onto CZrP

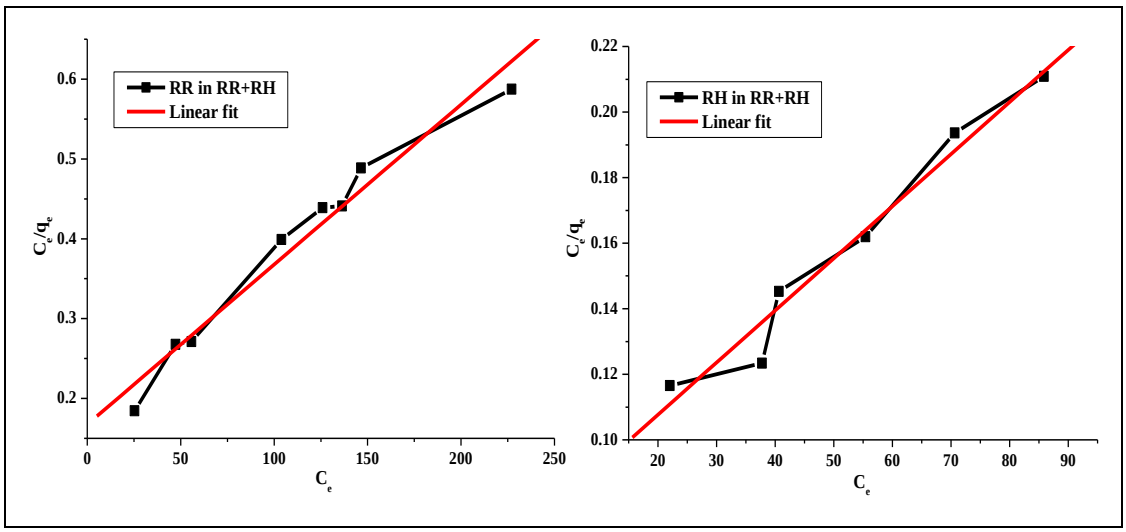

Operating parameters: 180 rpm, 100 ppm of dye, 0.05 g adsorbent, time 210 min, temperature 30^0C, optimum pH-9

Figure 5.19 c. Linear fit of isotherm for RR and RH in (RR+RH) onto CZrP

Table 5.4 Langmuir Isotherm constants for binary systems

Langmuir isotherm constants for binary systems								
	Binary component system ((RR+RB)							
	ZrP				CZrP			
RB+RR								
	K_l	a_l	q_m ($mg.g^{-1}$)	r^2	K_l	a_l	q_m ($mg.g^{-1}$)	r^2
RB	2.590	0.007	334.44	0.990	5.0666	0.01368	370.37	0.986
RR	10.706	0.0236	396.75	0.985	9.361	0.0223	436.65	0.991
P-factor	1.375		1.574		1.286		1.324	
RR+RH								
RR	3.259	0.0088	369.00	0.991	5.976	0.016	357.14	0.9833
RH	11.657	0.0277	420.16	0.976	13.18	0.035	435.23	0.9843
P-factor	1.213		1.763		1..276		1.732	
RB+RH								
RB	10.230	0.0333	306.74	0.9821	11.195	0.026	429.18	0.9773
RH	14.376	0.0339	423.72	0.9821	13.365	0.028	439.26	0.9223
P-factor	1.342		1.531		1.834		1.321	

Table 5.5 Parameters of Jain and Snoeyink modified extended Langmuir model.

ZrP			**Q_m ($mg.g^{-1}$)**	**% of dye adsorbed without competitive adsorption**
1.	RB+ RR	RB	353	50.99
		RR	180	49.01
2.	RR + RH	RR	386	36.79
		RH	142	63.21
C-ZrP			**Q_m ($mg.g^{-1}$)**	**% of dye adsorbed without competitive adsorption**
1.	RB+ RR	RB	294	43.54
		RR	128	56.46
2.	RR + RH	RR	306	37.91
		RH	116	62.09

Sorption kinetics of binary system

The sorption kinetics of binary system was fitted to pseudo first order, pseudo second order and intra particle diffusion models. The adsorption kinetics was well explained by pseudo second order model (Table 5.6) for all the systems onto ZrP and CZrP. Figure. 5.20 (a, b& c) and 5.21 (a, b& c) shows the linear fit for isotherms of RB+RR, RB+RH and RB+RR onto ZrP and CZrP. The adsorption percentage reduced in the binary mixture which is in correlation with isotherms. Also the intraparticle diffusion indicated that the rate of the reaction is controlled by more than one step.

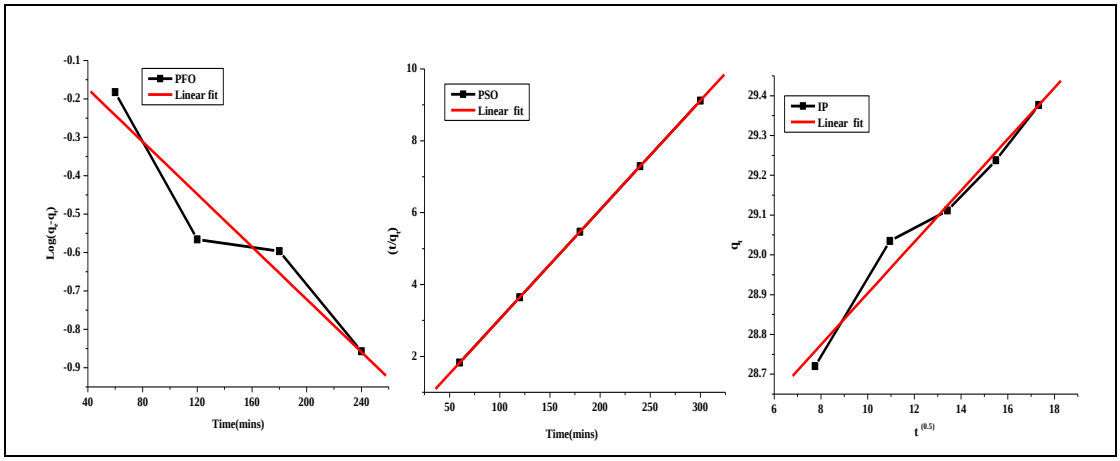

Operating parameters: 180 rpm, 100 ppm of dye, 0.05g adsorbent, time 210 min, temperature 30^0C, optimum pH

Figure 5.20 a. Linear fit of Kinetics for (RB+RR) onto ZrP

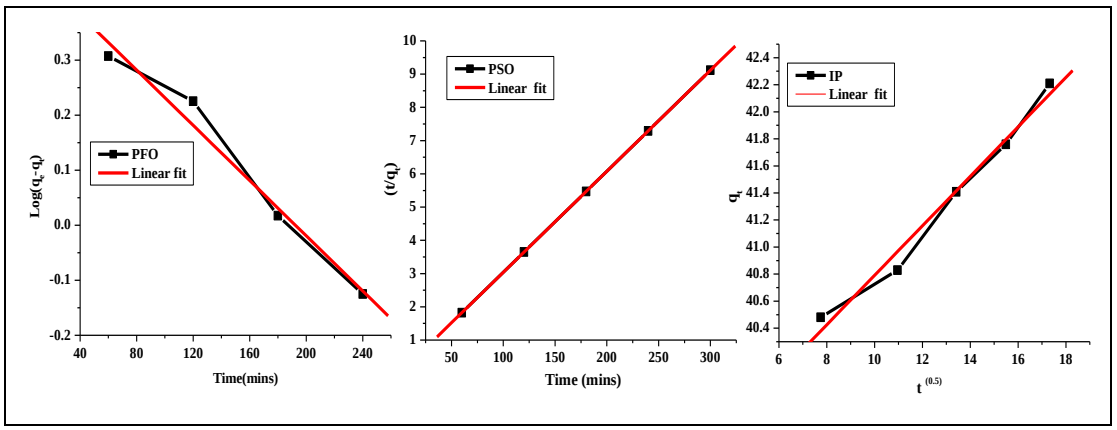

Operating parameters: 180 rpm, 100 ppm of dye, 0.05g adsorbent, time 210 min, temperature 30^0C, optimum pH

Figure 5.20 b Linear fit of Kinetics for (RB+RH) onto ZrP

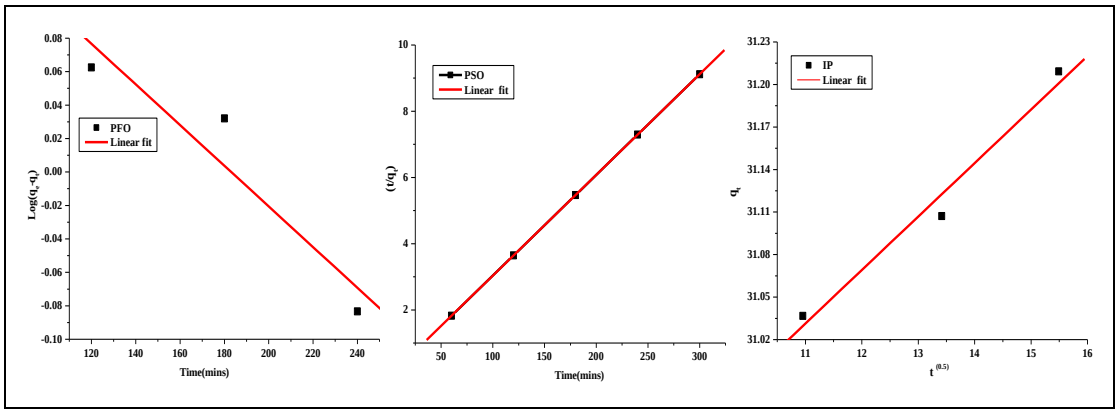

Operating parameters: 180 rpm, 100 ppm of dye, 0.05 g adsorbent, time210 min, temperature 30^0C, optimum pH

Figure 5.20 c. Linear fit of Kinetics for (RR+RH) onto ZrP

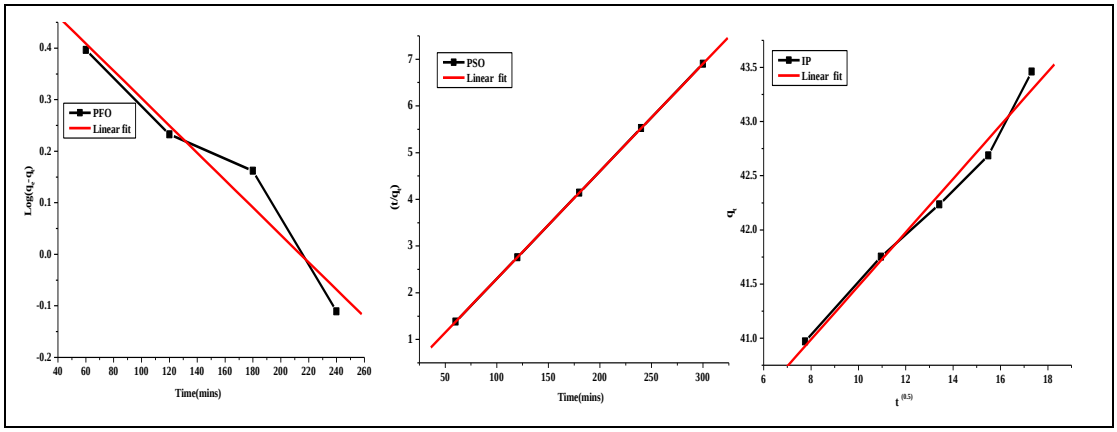

Operating parameters: 180 rpm, 100 ppm of dye, 0.05 g adsorbent, time210min, temperature 30^0C, optimum pH

Figure 5.21 a. Linear fit of Kinetics for (RB+RR) onto CZrP

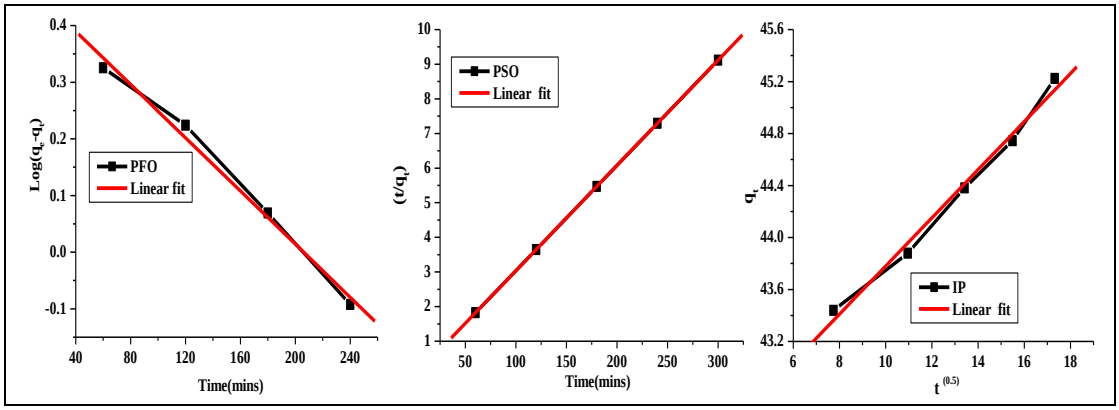

Operating parameters: 180 rpm, 100 ppm of dye, 0.05 g adsorbent, time 210 min, temperature 30^0C, optimum pH

Figure 5.21 b. Linear fit of Kinetics for (RB+RH) onto CZrP

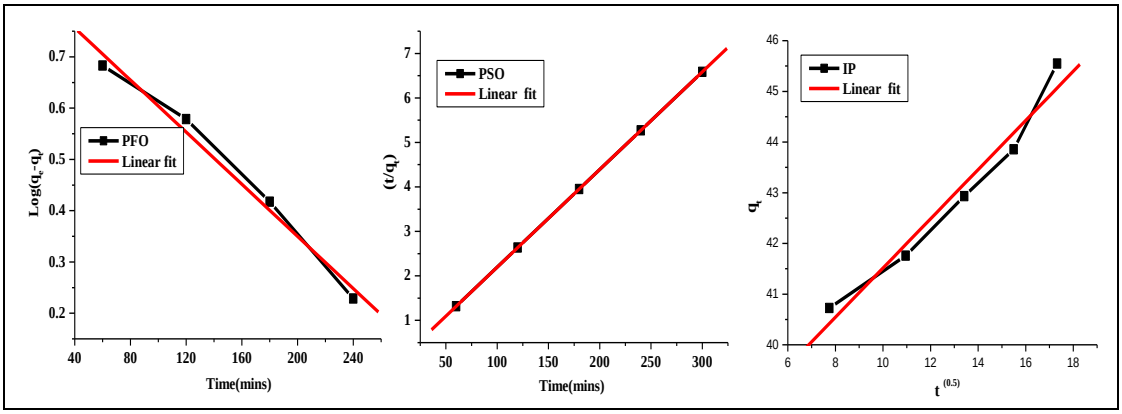

Operating parameters: 180 rpm, 100 ppm of dye, 0.05 g adsorbent, time 210 min, temperature 30^0C, optimum pH

Figure 5.21 c. Linear fit of Kinetics for (RR+RH) onto CZrP

Table 5.6 Kinetic constants for binary systems

Kinetics	**ZrP**			**CZrP**		
	RB+RR	RB+RH	RR+RH	RB+RR	RB+RH	RR+RH
Pseudo first order						
q_e (exp) ($mg.g^{-1}$)	36.54	32.18	37.87	42.12	41.54	43.76
q_e ($mg.g^{-1}$)	4.262064	3.038295	1.669283	4.963557	3.044388	7.210909
K_1 ($L.mmol^{-1}$)	6.63E-04	5.78E-03	2.81E-03	2.03E-02	5.41E-03	5.85E-03
r^2	0.9035	0.98804	0.9477	0.9035	0.99492	0.9923
SD	0.01295	0.03714	0.0347	0.01295	0.02251	0.03009
Pseudo Second Order						
q_e ($mg.g^{-1}$)	32.90	33.63	34.76	43.459	42.90	45.56
K_2 ($L.mmol^{-1}$)	6.20E-03	1.10E+11	1.01E+08	7.67E+07	1.10E+11	4.39E+07
r^2	1	1	1	1	1	1
SD	3.16E-10	3.16E-10	3.16E-10	3.65E-10	3.16E-10	3.16E-10
Intraparticle Diffusion						
K_{ip} ($L.mmol^{-1}$)	0.0651	0.9904	0.03773	0.24725	0.18517	0.00254
r^2	0.983	0.983	0.98806	0.9909	0.99407	0.98806
SD	0.3969	0.11055	0.0189	0.14608	0.99407	0.0189

5.3.10 Degradation of individual and binary mixture of dyes

The degradation of single (RB-21, RR-141 and Rh-6G) and binary mixture of dyes (RB+RR, RB +RH and RR+RH) was studied using ZrP and CZrP as a catalyst in the presence of H_2O_2 at room temperature. Figure 5.22 and figure 5.23 shows the UV spectra for degradation of individual dyes. It was observed that 99% of RB-21, 92 % of RR-141 and 90% of Rh-6G degraded in the presence of ZrP as catalyst while improved degradation was observed with CZrP as catalyst (99% of RB-21, 97 % of RR-141 and 96% of Rh-6G). In binary mixture of dyes (Figure 5.24 & 5.25) in the case of RB+RH and RB+RR, it was observed that Reactive blue-21 is completely degraded, and a very less amount of the other component is left undegraded (visually seen). In the case of RR+RH, Reactive red-141 is completely degraded leaving a small amount of undegraded Rhodamine6G (visually seen) in the mixture. Blank experiments were also done to check the catalytic activity of only H_2O_2 in the absence of catalyst and it was observed that H_2O_2 does not play any role in the degradation of dyes. This investigation of mixture of dyes can be compared with real effluents. The colourless solution after degradation was analyzed for TOC to see the extent of demineralisation. The decrease in TOC was more or comparable to other catalysts reported in literature [51]. The catalyst was washed and dried at room temperature for further degradation experiments. The catalyst was efficient for three cycles (figure 5.26). The rate of degradation was faster on comparison to adsorption and the percentage of adsorption of Rh–6G is high where as in degradation the percentage is less which is due the difficulty in breaking or decomposing the linkages present in the dye molecules.

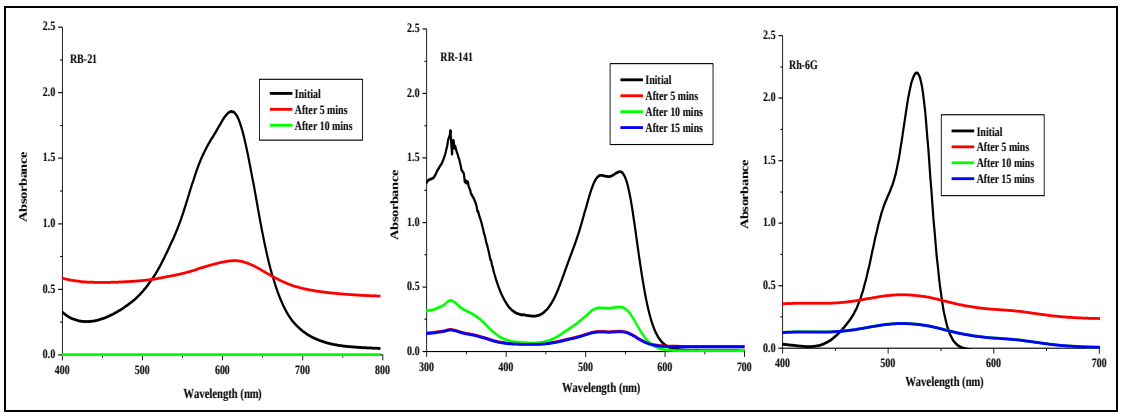

Operating parameters: 100 ppm of dye, 0.05 g of catalyst, temperature 30^0C, pH6

Figure 5.22 Degradation of individual dyes at Room temperature in the presence of H_2O_2 using **ZrP as a catalyst**

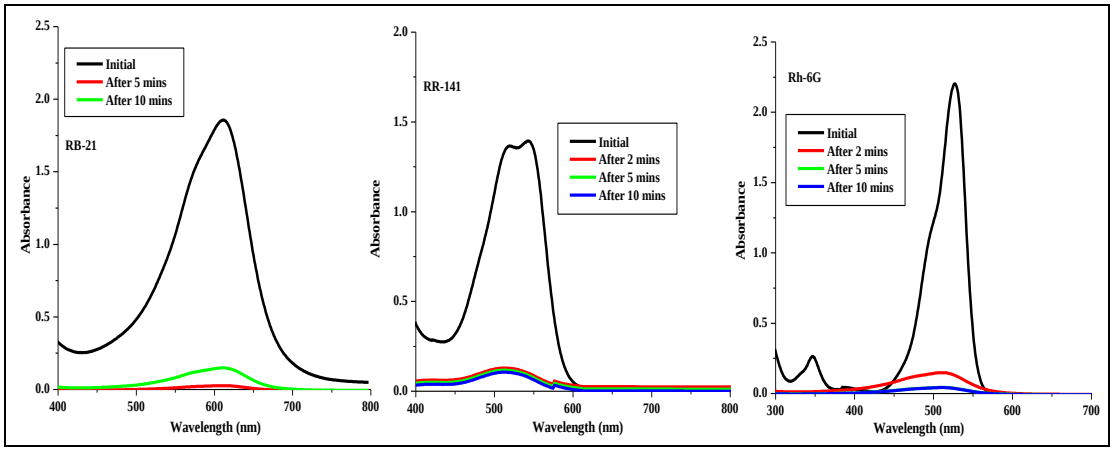

Operating parameters: 100 ppm of dye, 0.05 g of catalyst, temperature 30^0C, pH-6

Figure 5.23 Degradation of individual dyes at Room temperature in the presence of H_2O_2 using CZrP as a catalyst

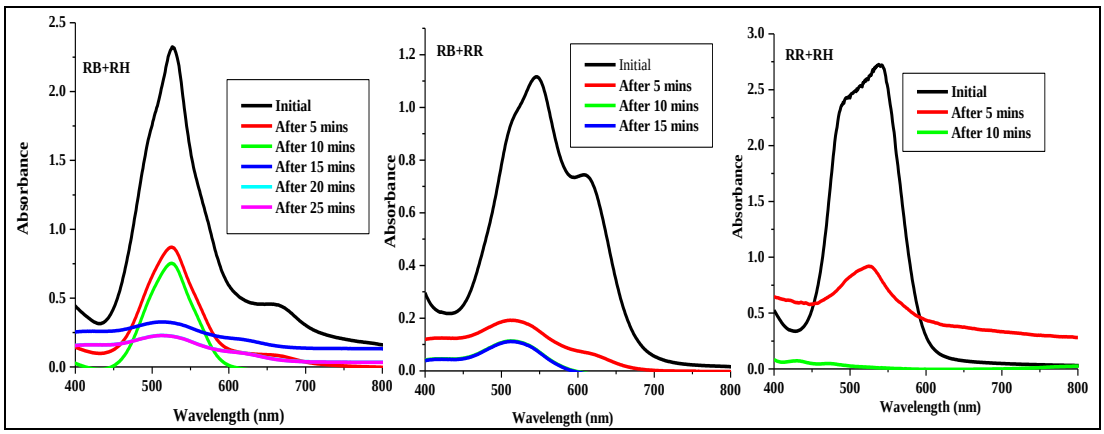

Operating parameters: 100 ppm of dye, 0.05 g of catalyst, temperature 30^0C, pH-6

Figure 5.24 Degradation of mixture of dyes at Room temperature in the presence of H_2O_2 using ZrP as a catalyst

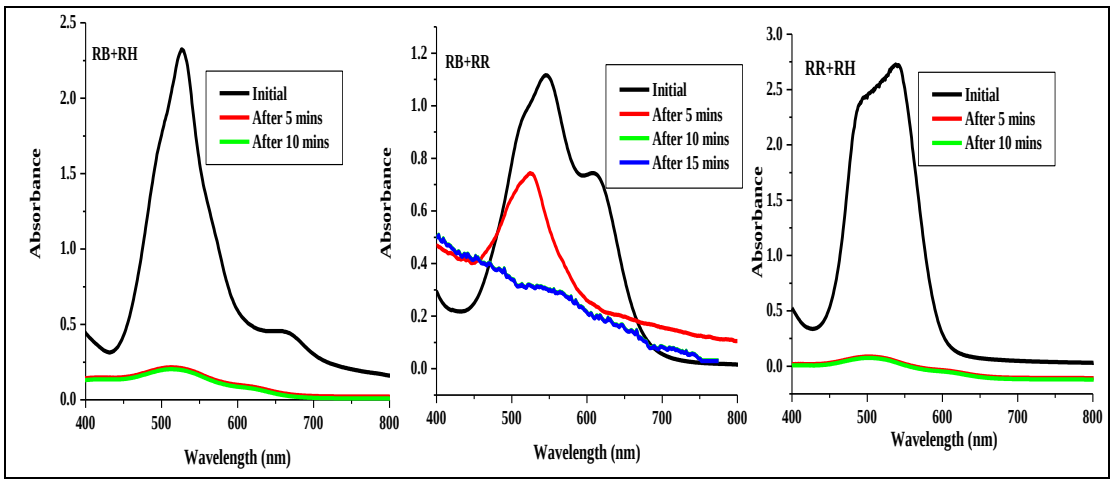

Operating parameters: 100 ppm of dye, 0.05 g of catalyst, temperature 30^0C, pH-6

Figure 5.25 Degradation of mixture of dyes at Room temperature in the presence of H_2O_2 using CZrP as a catalyst

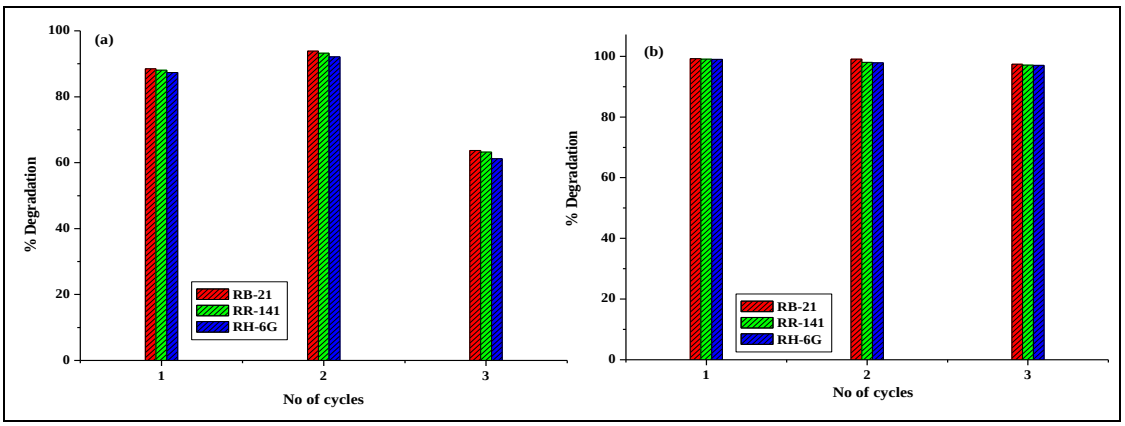

Figure 5.26 Catalyst reusabilty studies

5.3.11. Total organic content

Figure 5.27 shows the TOC reduction for individual and binary mixture of dyes. The mineralization of organic carbon of the dyes in single component systems or in binary components was investigated by the Total Organic Carbon (TOC) measurements. It was observed that there was 58%, 44% and 77% reduction in TOC for RB-21, RR-141 and Rh6G for ZrP in single component systems and 39%, 44% and 47% for binary system RB+RH, RR+RH and RB+RR respectively for ZrP. In the case, CZrP the TOC reduction was 41%, 21% and 19% for single component system and 8%, 22% and 23% for binary systems of RB+RH, RR+RH and RB+RR

respectively. The TOC reduction is lesser than decolorization which may be due to the formation of smaller uncolored products.

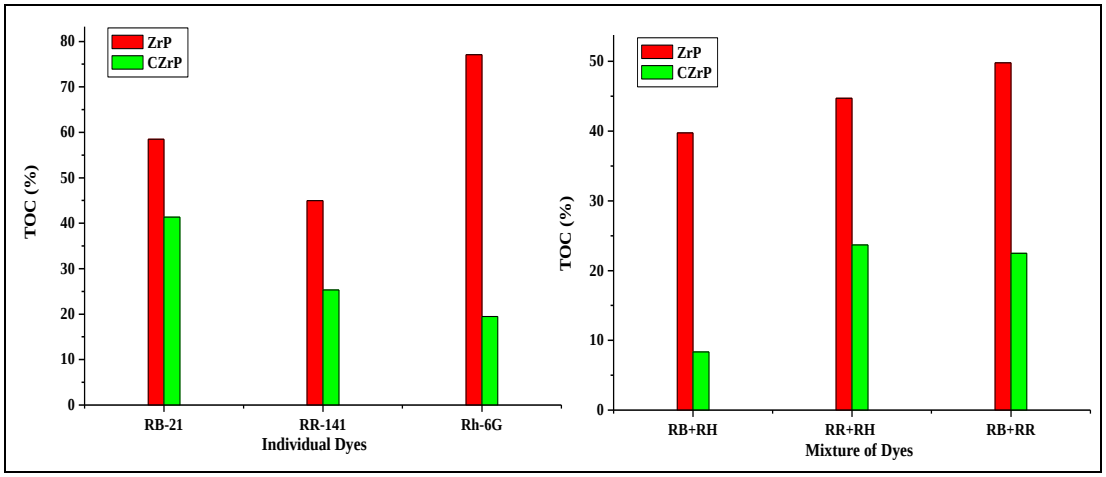

Figure 5.27 TOC for individual and binary mixture of dyes

5.3.12 Discussion

The interaction of H_2O_2 and a protic solvent, water, with the Zr active site in Zirconium phosphate could result in the formation of peroxo-zirconium species [52]. The disproportionation of the peroxide to oxygen and water could be catalyzed at the interface, as indicated by the substantial formation of oxygen. The liberation of oxygen could be visually seen when ZrP and CZrP are in contact with H_2O_2. However superoxide and $^{\cdot}OH$ and $HO_2^{\cdot}$ radicals are intermediate of the disproportionation of H_2O_2 which could be transferred to the dye resulting in oxidation of the dye.

5.4. Conclusion

Chitosan-Zirconiumphosphate nanocomposites an efficient adsorbent for removal ofindividual and binary mixture of cationic and anionic dyes (RB-21, RR-141 and Rh-6G). The X-ray diffraction pattern shows that the nanocomposite has intercalation and exfoliation in the structure. The Freundlich constant, 1/n was less than unity implied that the adsorption intensity was favorable over the entire range of concentrations studied for all the adsorbents. The positive values of ΔGindicate the non-spontaneous nature of adsorption. The adsorption kinetics data fitted well with the pseudo-second-order kinetic model. Chitosan-Zirconium phosphate nanocomposite showed higher adsorption capacity for both cationic and anionic dyes reflecting a promising future for the utilization of the nanocomposite as an adsorbent for removal of dyes from aqueous solution. In addition to adsorption the nanocomposite was explored for its catalytic degradation of single and binary mixture

of dyes due to its ability to form peroxo complexes which could catalyze the degradation of dyes.

References

[1] a) G. Alberti, U. Costantino, in Intercalation Chemistry, (Eds: M. S. Whittingham, A. J. Jacobson), Academic, San Diego, CA (**1982)**, 147

b) A. Clearfield, U. Costantino, in Comprehensive Supramolecular Chemistry, Vol. 7 (Eds: G. Alberti, T. Bein), Elsevier, Amsterdam **(1996)** 107.

[2] T. A. Saleh, V. K. Gupta, *Environ. Sci. Pollut. Res.*19 **(2012)** 1224.

[3] F. S. Asghari,H. Yoshida, *Carbohydr.Res.* 341 **(2006)**2379.

[4] B. C.Pan, et al. *Water Res*. 41 **(2007)** 3103.

[5] L. Wang et al.,*ACS Appl. Mater. Interfaces* 4**(2012)** 2686.

[6] S. K. Swain et al.,*Chem. Eng. J.* 171**(2011)**1218.

[7] O. P. Panwar, A. Kumar, R. Ameta, S. C. Ameta, *Chem. Eng. J.* 27**(2008)**133.

[8] Z. Barhon, A. Albizane,M. Azzi, N. Saffaj, J. Bennazha, S. A. YoUnssi, *J. Appl. Sci. Res.* 5**(2009)** 893.

[9] R. Hoppe, G. Alberti, U. Costantino, C. Dionigi, G. S. Ekloffand, R. Vivani, *Langmuir* 13**(1997)** 7252.

[10] A. Jayswal, U. Chudasama, *Indian J. Chem. Technol.* 14 **(2007)**597.

[11] M. H. Hussein, Alhendawi, *J. Mater. Chem*. 21 (**2011**)7748 .

[12] E. P. Giannelis, *Adv. Mater.* 8 **(1996)** 29-35.

[13] P. C. Lebaron, Z. Wang, T. J. Pinnavaia, *Appl. Clay Sci.*15**(1999)**11.

[14] M. Alexandre, P. Dubois, *Mater. Sci. Eng.*28 **(2000)**1.

[15] T. J. Pinnavaia, G. W. Beall, *Polymer–Clay Nanocomposites*, **(2000)**.

[16] Q. Zhang, Q. Du, T. Jiao, Z. Zhang, S. Wang, Q. Sun, F.Gao, Scientific Reports. 3 2551.

[17] H. J.Sue, K. T. Gam, N. Bestaoui, N. Spurr, A. Clearfield, *Chem. Mater.* 16**(2004)**242.

[18] R. Zhang, Y. Hu, B. Li, Z. Chen,W.Fan,*Journal of Materials* 42 **(2007)** 5641.

[19] L. Liu , J. Wen, L. Liu, D. He, R.Kuang, T. Shi, *Anal Biochem.* 445 **(2014)** 24.

[20] Polymer International 59 **(2010)** 923

[21] Amphlett, C. B. *Inorganic Ion Exchangers*; Elsevier: Amsterdam, 1964.

[22] P.Wu, Y. Liu, M. He, M. Iwamoto, *Chem. Mater*. 17**(2005)**3921.

[23] A. Sinhamahapatra, N. Sutradhar, B. Roy, A. Tarafdar, H. C. Bajaj, A. B. Panda, *Appl. Catal. A* 385**(2010)** 22.

[24] K. N. Rao,A. Sridhar,A. F. Lee, S. J. Tavener, N. A. Young, K. Wilson, *Green Chem*. 8 **(2006)**790–797. ,

[25] Swapan K. Das, Manas K. Bhunia, Anil K. Sinha, and AsimBhaumik, ACS Catal. 1**(2011)** 493–501

[26] J. A. Connor, E. A. V. Ebsworth, in:*Advances in Inorganic Chemistry and Radiochemistry*, Academic Press,6 **(1964)** 279. New York,

[27] R. E. Connick, W. H. McVey, *J. Am. Chem. Soc.**71*** **(1949)**3182.

[28] S. E. Horsley, D. V. Nowell, D. T. Stewart, *Spectrochim. Acta, Part A,* 30 **(1974)** 535

[29] *J. Chem. SOC., Faraday Trans. 1*83 **(1987)** 853.

[30] Z.-Y. Yuan et al., *Catalysis Today* 105 **(2005)** 647

[31] L. Wang, X. Wu, W. Xu, X. Huang, J. Liu, A. Xu, *ACS Appl. Mater. Interfaces* 4**(2012)** 2686.

[32] *J. Mater. Chem.* 16**(2006)** 759

[33] M Anpo et al, *J chem. Soc Fraday transactions* 84 **(1988)** 751

[34] L. Wang, X. Wu, W. Xu, X. Huang, J. Liu, A. Xu, *ACS Appl. Mater. Interfaces* 4**(2012)** 2686.

[35] L. Y. Sun, W. J. Boo, R. L. Browning, H. J. Sue, A. Clearfield, *Chem. Mater*. 17**(2005)** 5606.

[36] L. Sun, W. J. Boo, H. Sue, A. Clearfield, *New J. Chem.*31 **(2007)** 39.

[37] G. Alberti, *Accounts Chem. Res.*11 **(1978)** 163.

[38] A. Clearfield, *Annu. Rev. Mater. Sci.* 14**(1984)**205.

[39] A. Clearfield, *J. Mol. Catal* 1984, 27 (1-2), 251−262.

[40] G. Alberti, *Accounts Chem. Res.*11 **(1978)** 163.

[41] A. Clearfield, *Annu. Rev. Mater. Sci.* 14**(1984)**205.

[42] A. Clearfield, *J. Mol. Catal* 1984, 27 (1-2), 251−262.

[43] L Sue, A. Clearfield, *New J. Chem.* 31 **(2007)** 39. Sun,W. J. Boo, H.

[44] H. Hu, J. C. Martin, M. Xiao, C. S. Southworth, Y. Z. Meng, L. Y. Sun, *J. Phys. Chem.C*, 115 **(2011)** 5509.

[45] W. J. Boo, L. Sun, J. Liu, A. Clearfield, H. J. Sue, *J. Phys. Chem. C* 2007, 111 (28), 10377−10381.

[46] G. Alberti, M. Casciola, D. Capitani, A. Donnadio, R. Narducci, M. Pica, M. Sganappa, *Electrochim. Acta*, 52 **(2007)** 8125.

[47] H. Hu, J. C. Martin, M. Zhang, C. S. Southworth, M. Xiao, Y. Z. Meng, L. Y. Sun, *RSC Adv.* 2**(2012)**3810.

[48] L. Y. Sun, W. J. Boo, D. H. Sun, A. Clearfield, H. J. Sue, *Chem. Mater.* 19 **(2007)**1749

[49] P. N. Kumar, S. Kannan, *RSC Adv*.4 **(2014)** 29946.

[50] K.Y. Foo, B.H. Hameed, *Chem. Eng. J.* 156 **(2010)** 2.

[51] Veda Ramaswamy, Bhavana Tripathi, D. Srinivas, A. V. Ramaswamy, Ricardo Cattaneo and Roel Prins *Journal of Catalysis*200**(2001)**250

[52] *Materials Chemistry and Physics,* 29 **(1991)** 379-386.